Accounting for the fringe magnetic field from the bending magnet in a Monte Carlo accelerator treatment head simulation

Tuathan P O'Shea[1, 2], Mark J Foley[1] and Bruce A Faddegon[2]

[1] School of Physics, National University of Ireland Galway, University Road, Galway, Ireland

[2] University of California San Francisco Comprehensive Cancer Center, 1600 Divisadero Street, San Francisco, CA 94143-1708, USA

E-mail: mark.foley@nuigalway.ie

ABSTRACT

Purpose: Monte Carlo (MC) simulation can be used for accurate electron beam treatment planning and modeling. Measurement of large electron fields, with the applicator removed and secondary collimator wide open, has been shown to provide accurate simulation parameters, including asymmetry in the

measured dose, for the full range of clinical field sizes and patient positions. Recently, disassembly of the treatment head of a linear accelerator has been used to refine the simulation of the electron beam, setting tightly measured constraints on source and geometry parameters used in simulation. The simulation did not explicitly include the known deflection of the electron beam by a fringe magnetic field from the bending magnet which extends into the treatment head. Instead, the secondary scattering foil and monitor chamber were unrealistically laterally offset to account for the beam deflection. This work is focussed on accounting for this fringe magnetic field in treatment head simulation.

Materials & Methods: The magnetic field below the exit window of a Siemens Oncor linear accelerator was measured with a Teslameter from 0 - 12 cm from the exit window and 1 - 3 cm off-axis. Treatment head simulation was performed with the EGSnrc / BEAMnrc code, modified to incorporate the effect of the magnetic field on charged particle transport. Simulations were used to analyze the sensitivity of dose profiles to various sources of asymmetry in the treatment head. This included the lateral spot offset and beam angle at the exit window, the fringe magnetic field and independent lateral offsets of the secondary scattering foil and electron monitor chamber. Simulation parameters were selected within the limits imposed by measurement uncertainties. Calculated dose distributions were then compared with those measured in water.

Results: The magnetic field was a maximum at the exit window, increasing from 0.006 T at 6 MeV to 0.020 T at 21 MeV and dropping to approximately 5% at the secondary scattering foil. It was up to 3 times higher in the bending plane, away from the electron gun, and symmetric within measurement uncertainty in the transverse plane. Simulations showed the magnetic field resulted in an offset of the electron beam of 0.80 cm (average) at the machine isocenter for the exit window only configuration. The fringe field was responsible for up to 7.6% asymmetry and 0.3 cm (average) offset of the clinical beam R_{max} profiles. With the magnetic field included in simulations, a single (realistic) position of the secondary scattering foil and monitor chamber was selected. Measured and simulated dose profiles showed agreement to an average of 2.5% / 0.16 cm (maximum: 3% / 0.2 cm), which is a better match than previously achieved without incorporating the magnetic field in the simulation. The undulations from the 3 stepped layers of the secondary scattering foil, evident in the measured profiles of the higher

energy beams, are now aligned with those in the simulated beam. The simulated fringe magnetic field had negligible effect on the central axis depth dose curves and cross-plane dose profiles.

Conclusion: The fringe magnetic field is a significant contributor to the electron beam in-plane asymmetry. With the magnetic field included explicitly in the simulation, realistic monitor chamber and secondary scattering foil positions have been achieved, and the calculated fluence and dose distributions are more accurate.

I. INTRODUCTION

Monte Carlo treatment head and patient simulation is a preferred method of accurate electron dose calculation in conformal electron and mixed beam therapy techniques[1,2] and also has potential to improve beam models employed in commercial treatment planning software.[3, 4, 5] Large electron fields, with the applicator removed and secondary collimators wide open, have been employed, in varying degrees of detail, for simulation of the treatment head of linear accelerators from various manufacturers including Varian[6, 7], Elekta[8] and Siemens.[9, 10] Disassembly of a Siemens Oncor treatment head was used to further constrain source and treatment head geometry simulation parameters.[11, 12] In that work, a fringe magnetic field from the bending magnet downstream of the exit window (with magnitude up to 0.02 T) was found to displace the electron beams by up to 0.9 cm at isocenter. The secondary scattering foil and monitor chamber in the simulation were unrealistically laterally offset from the collimator rotation axis, to match the measurement asymmetry, without simulation of the fringe field. The current work focusses on characterizing this fringe magnetic field and including the field in Monte Carlo treatment head simulations with the goal of improving the accuracy of the calculated fluence and dose distributions.

II. MATERIALS AND METHODS

II.A. Siemens Oncor accelerator

The Siemens Oncor (Concord, CA) is a S band (2856 MHz) standing wave electron accelerator providing six clinical electron beams in the energy range 6 – 21 MeV. Megavoltage beams are produced in a horizontally mounted (copper) waveguide and a 270° bending and focusing magnet system[13] (Stangenes Industries Inc, Palo Alto, CA) is employed to transport the electron beam into the treatment head. This magnet consists of two low carbon steel pole pieces fitted with two "D" shaped electromagnets. The vacuum envelope occupies a 1.78 cm gap between the poles and acts as a ± 7% width energy filter. The envelope mean radius is approximately 6 cm, requiring a field of over 1 T to bend the highest energy beam onto the exit window. Each pole face can be divided into 5 regions (figure 1): (1) the entrance pole face edge, (2) constant field region, (3) focusing gradient region, (4) constant field region and (5) exit pole face edge. The entrance and exit pole faces are angled and have extended fringe fields which are important in beam focusing.

After transport through the magnet, the electron beam enters the treatment head through a water-cooled titanium exit window. The inplane position of the electron spot on the exit window (spot offset, $x_{S,Y}$) is controlled via two orthogonal dipoles surrounding the waveguide. The current in these steering coils is preset for each beam energy to centralize the electron beam on the exit window and to optimize beam uniformity (which is monitored downstream by the electron monitor chamber). The internal machine parameter defining the current flowing through these coils is called STCI and is given in milliamperes (STCI ≈ 900 mA for the nominal 21 MeV beam). Faddegon et al. (2009) showed the steering coils on the waveguide moves the beam ($x_{S,Y}$) inplane 0.1 – 0.2 cm per ampere.[11] Adjusting the beam energy shifts the spot position at the exit window in the inplane direction.

After entering the treatment head, the beam is scattered by primary and secondary scattering foils before traversing a monitor ionization chamber. The primary foil is enclosed in a brass holder with a stainless steel retainer. The wall of the monitor chamber collimates the beam to a 36 cm diameter field size at isocenter. For the largest field (40×40 cm^2) with

no applicator, the position of the field edges are determined by the lateral position of the monitor chamber. The lateral position of the aluminium secondary scattering foil is a critical component in determining the flatness and symmetry of the electron beam. The fringe magnetic field extends into the space between the exit window and monitor chamber, modifying the spatial and angular characteristics of the beam.

II.B. Measurements

II.B.1. Water tank scans

Measured lateral dose profiles and percentage depth dose curves used in this work have been reported previously.[11] Measurements were taken on a Siemens Oncor linac for 6 – 21 MeV electron beams and 3 different treatment head configurations: (1) exit window only in the beam, (2) primary foil added and finally (3) full clinical head with the secondary foil and monitor chamber in the beam line (figure 1). The applicator was removed and jaws and MLC set to maximum (40×40 cm^2) field size for all configurations with a source-to-surface distance (SSD) of 100 cm. Dose profiles were measured with a CC13 (Scanditronix–Wellhöfer, Uppsala, Sweden) thimble ionization chamber centered on the collimator rotation axis. Profiles were measured at the depth of dose maximum, R_{max}, and in the bremsstrahlung tail, R_x. Percentage depth ionization was measured with a Roos parallel plate chamber (N34401, PTW, Freiberg, Germany) with an effective point of measurement (EPOM) of 0.115 cm, and percentage depth dose with an EFD diode (Scanditronix–Wellhöfer, Uppsala, Sweden) with 0.045 cm EPOM correction. The lateral offset of the secondary scattering foil and electron monitor chamber, from the collimator rotation axis, was estimated from digital photographs. The uncertainty in the offsets was estimated as ± 0.03 cm. These positions were used for quality control and to guide selection of simulation offsets.

II.B.2. Magnetic field measurements

With the linac in electron mode, the monitor chamber and secondary scattering foil were removed to allow access to the region below the exit window. The bending magnet was energized with currents of 13.1 – 42.2 A which covered the nominal energy acceptance range of 6 – 21 MeV. The magnetic field below the exit window was measured with a Tesla meter (F.W. Bell model 4048, Milwaukie, OR). The meter had a resolution of 0.01×10^{-3} T and an accuracy specification of ± 2%. The Hall probe had dimensions: 0.419 cm × 0.145 cm × 6.35 cm. With the bending magnet energized, the probe flat was aligned with the north magnetic field which entered from the positive crossplane (perpendicular to the electron gun) direction. Measurements were taken 12 cm along the central axis and up to 3 cm off-axis at 1 cm intervals. There is restricted space in the treatment head, such that, measurements further off-axis (than those reported) were not possible in most cases. The estimated uncertainty in the measured magnetic field measurements was 17%. This included the accuracy specification (±2%) and estimates of positioning uncertainty (±3 mm), orientation (±5°) and reproducibility of three measurements (±8%), added in quadrature.

II.C. Monte Carlo simulations

II.C.1. Simulation codes

Monte Carlo treatment head simulation was performed with EGSnrc (version 1.4)[14] / BEAMnrc (version 1.104)[15] for the three different treatment head configurations outlined in section II.B.1: (1) exit window only, (2) primary foil and (3) clinical beam. Phase space data was scored at 100 cm SSD. Dose-to-water was calculated using MCRTP[16] with a 40 × 40 × 20 cm^3 phantom containing 0.2 × 0.2 × 0.1 cm^3 voxels. 800 million incident source electrons were tracked to achieve uncertainty in subsequent dose calculations of 1%. Transport parameters were the same as used in previous Siemens Oncor electron head simulations.[11, 12]

II.C.2. Incident electron source

The electron source incident on the exit window was characterized by six parameters: (1) mean energy, E, (2) Gaussian energy spread, $\phi'(E)$, (3) Gaussian (spot) spatial distribution, r_S, (4) spot offset from collimator rotation axis, x_S, (5) beam angle, Θ and (6) angular divergence, $\phi'(\Theta)$. The mean energy (E) and Gaussian energy spread ($\phi'(E)$) were previously selected to match the measured depth of 50% ionization, I_{50} and the slope of the fall-off portion of the PDI curve, respectively, with the primary foil only in the beam.[12] The fringe magnetic field below the exit window has a negligible effect on these parameters, demonstrated in section III.C. Mean energies (E) of 6.69 MeV, 9.69 MeV, 12.38 MeV, 15.85 MeV, 19.57 MeV and 21.75 MeV were used for the nominal 6 – 21 MeV electron beam with $\phi'(E)$ of ± 7.1%, ± 4.9%, ± 6.2%, ± 6.0%, ± 4.8% and ± 3.3%, respectively, consistent with the approximate ± 7% transmission bandwidth of the vacuum envelope.[13]

A Gaussian spatial distribution, r_S, of 0.2 cm was used.[6, 17] Increasing the electron beam radius from 0.1 cm to 0.2 cm was previously found to have very little effect, typically below 1%.[18] Electron dose distributions are insensitive to r_S values in the realistic range of 0.1 – 0.3 cm. The spot offset (x_S) and beam angle (Θ) were previously measured.[11] An analysis of the experimental uncertainty associated with both of these parameters was performed and each parameter was then allowed to vary within these tolerances. The experimental uncertainty in x_S was estimated to be no more than ±0.05 cm. The beam angle, which was based on the position of the peak of the profile in the bremsstrahlung tail, had larger experimental uncertainty for lower energies which generate less bremsstrahlung x-rays and therefore a less detectable peak (figure 2). The experimental uncertainties in the beam angles (directional cosines) were estimated as ±0.52° (0.009), ±0.34° (0.006), ±0.17° (0.003), ±0.11° (0.002), ±0.09° (0.0015) and ±0.09° (0.0015) for the nominal 6 - 21 MeV beams, respectively.

II.C.3. Treatment head simulation including fringe magnetic field

An electron in a vacuum with applied magnetic field travels in a curved path dictated by the Lorentz force. The radius of curvature of the electrons path is given by:

$$R = \frac{\gamma m v}{eB} \quad (1)$$

where γ is the Lorentz factor, m is the electron mass = $9.10938188 \times 10^{-31}$ kg, v is velocity of the particle perpendicular to the magnetic field, e is the electron charge = $1.60217646 \times 10^{-19}$ C and B is the magnetic field in Tesla. From equation 1, the maximum fringe field value measured below the exit window (0.006 - 0.020 T) would result in radius of 3.6 m for electrons with nominal energies of 6 – 21 MeV.

Monte Carlo treatment head simulation was performed with a modified version of BEAMnrc (version 1.104) which accounted for the effect of the lateral shift of components. Electron beam transport in the presence of a magnetic field made use of the generalized *emf_macros.mortran* macro package originally developed for EGS4.[19] This has been used for various applications with magnetic fields in the range of 0.1 – 20.0 T.[19, 20, 21, 22]

The EMF macros treat scattering and magnetic field deflections as independent processes. Velocity changes resulting from magnetic field deflection are added at the end of each conventional charged particle transport step. This implementation requires step-size restrictions. The step sizes within the condensed history algorithm must be sufficiently short so that the relative change in the particles direction of motion is small. From the macros, step size is restricted to $0.02\ m\,c^2 / (100\ |B_{perp}|\ e\ c)$ cm or less, where $m\,c^2$ is electron rest mass, c is speed of light, e is the electron charge and $|B_{perp}|$ is the magnitude of the magnetic field in Tesla.[22] For electrons travelling perpendicular to the magnetic field the step size should be restricted to approximately 1.7 cm for the maximum field measured at the exit window (0.02 T). Kirkby et al. (2008) showed PENELOPE and EGSnrc dose distributions generally agreed

to within statistical uncertainty (~1%) for slab phantoms with applied magnetic fields of 0.2 and 1.5 T.[22] Simulations were performed to ensure that the code could adequately simulate electron trajectories in simple geometries with reasonable accuracy. EGSnrc was found to accurately simulate the deflection of mono-energetic pencil beams, with initial kinetic energies of 6 – 21 MeV, over 10 cm with 0.1 T applied magnetic field. EGSnrc matched the 2.45 – 0.70 cm deflection predicted using equation 1 to within 0.1 – 0.05 cm for 6 – 21 MeV, respectively.

The fringe magnetic field was simulated using an in-house component module (CM): RECT, originally developed for dose calculation in a patient model. This component, consisting of a rectilinear array of voxels, allowed simulation of a region dependent magnetic field in the treatment head (a different field may be specified for each voxel, with the field constant within the voxel). The magnet field measured below the exit window (II.B.2) was used in the treatment head simulations. The RECT CM was positioned between the exit window and secondary scattering foil. The CM contained 1.0 cm^3 air regions, each with a corresponding magnetic field vector. The maximum electron transport step-size was not restricted to less than the region (voxel) dimensions, however, simulations were also performed with the maximum step-size reduced to 0.1 cm. This resulted in a neligible difference to the beam profile (in particular field size and offset) at isocenter.

The offset of the (y) jaws and (x) multi-leaf collimator, from the collimator rotation axis, were estimated from the field edge of the 18 MeV beam in primary foil only configuration. Peripheral material (tungsten MLC tracks and steel support structure) below the MLC bank was previously found to significantly collimate the edge of the 6 MeV field resulting in an over-estimation of the inplane field edge by up to 1.4 cm.[11] This material was included in the current study along with the fringe magnetic field simulation.

II.C.4. Sensitivity of clinical dose profiles to sources of asymmetry

The effect of various sources of electron beam asymmetry on idealized symmetric R_{max} dose profiles was investigated by Monte Carlo simulation. The incident electron beam (spot) offset, x_S, and angle (at the exit window), Θ, were varied by the experimental uncertainties reported in section II.C.2. The effect of secondary scattering foil and monitor chamber lateral offsets of 0.1 cm were also separately quantified, as well as, the effect of the (measured) fringe magnetic field. Sensitivity was quantified in terms of change in flatness ($\Delta_{Flatness}$), symmetry (Symmetry), field offset (of 50% dose points) and slope (($D_{12cm} - D_{-12cm}$)/24, % / cm) of line through points at +12 cm and -12 cm from the central axis. Flatness was defined as $100 \times (D_{max} - D_{min}) / (D_{max} + D_{min})$ and symmetry as the difference in dose at points +12 cm and -12 cm from the central axis ($D_{12cm} - D_{-12cm}$). The flatness of the idealized symmetric profiles ($Flat_{baseline}$) was 2.4%, 3.0% 0.35%, 1.7%, 2.8% and 6.65% for 6 – 21 MeV, respectively. The change in flatness (from baseline; $\Delta_{Flatness} = Flat_{new} - Flat_{baseline}$) was calculated and reported in the results section III.D.1.

III. RESULTS & DISCUSSION

III.A. Magnetic field measurements

The magnetic field at the exit window was found to increase from 0.006 T to 0.020 T with bending magnet current (beam energy), as expected, with a slope of 0.48 mT / A and intercept of -0.4 mT. The field was a maximum with the probe flat aligned with the crossplane (x) axis, perpendicular to the electron gun and along the axis of the magnet poles (figure 3). It dropped to ~0 T when the probe flat was aligned with the inplane (y) axis (in the plane of the gun).

The magnetic field along the central axis was maximum at the exit window, dropping to approximately 5% of this value at a distance of 12 cm (figure 4). There was a sharp drop in the magnetic field in the vicinity of the primary foil holder, approximately 1 cm from the exit

window. With the Hall probe fixed at the exit window, the holder was removed. The magnetic field was found to increase by up to 20%. The primary foil holder steel is likely high permeability (μ) which acts as a field shunt.[23] Monte Carlo simulations were performed with and without (by fitting a cubic function to the data excluding the point at 1 cm from the exit window) the drop in the fringe field. A comparison of exit window only R_{max} profiles showed negligible differences, however, it is likely that (a) the magnetic field measurements (performed every centimeter) did not have the required resolution to fully model the field in this area and (b) the field above and below the holder is also affected. Independently measured clinical beam profiles demonstrated the holder did affect the inplane symmetry, resulting in a 2-3% change in the off axis ratio. All subsequent measurements were performed with the holder in place – consistent with all three beam configuration.

Figure 5 shows the fringe magnetic field measured across the inplane (y) axis for the 21 MeV beam (42.2 A) and at 2 – 10 cm from the exit window. The magnetic field has a clear gradient; up to 3 times higher on the negative inplane (-y) side, with the same shape for 6 – 18 MeV beams. Linear regression was performed on the measured profiles at 3, 5, 7 and 9 cm distances (from the exit window) to highlight the gradient, which had slopes of 3.1, 1.5, 0.7 and 0.3 mT / cm, respectively. This gradient is due to the angled exit pole faces of the bending magnet discussed in section II.A. The magnetic field variation in the crossplane (x) direction was symmetric within the 17% uncertainty of the magnetic field measurements.

III.B. Exit window only configuration

Figure 6 compares measured and simulated R_{max} inplane dose profiles with the exit window only in the beam line for 6 – 21 MeV and 100 SSD. The measured inplane profiles were offset negative inplane (-y) from the collimator rotation axis by -1.16 cm, -1.14 cm, -1.00 cm, -0.99 cm, -0.87 and -1.16 cm, for 6 – 21 MeV, respectively. The (measured) fringe magnetic field was found to account for the majority of the offset, based on simulation results: -0.83

cm, -0.87 cm, -0.83 cm, -0.84 cm, -0.82 cm and -0.73 cm for 6 – 21 MeV. The spot offset (x_S) and beam angle (Θ) at the exit window accounted for the remainder of the offset.

The exit window water channel was thickened by 0.06 cm (19.3%) over manufacturer specification to match the 6 MeV R_{max} crossplane (x) FWHM. The exit window water channel is under pressure with a vacuum on one side, making it thicker than specified and angular divergence at the exit window is limited by the width of the profile in the bremsstrahlung tail.[17] A thinner water channel could be used with an increased angular divergence at the exit window, but this has negligible impact on the simulation through the remainder of the treatment head.

Angular divergence, $\phi'(\Theta)$, was added for each of the higher energy beams (9 - 21 MeV) to match the measured crossplane profile widths with the thicker water channel (Table 3). The required divergence increased with energy up to 15 MeV, where it was a maximum of 0.85° (crossplane) and 1.1° (inplane) and then decreases for higher energies. Measured inplane R_{max} profiles were 0.09 – 0.29 cm wider than corresponding crossplane profiles. Spatial dispersion is usually more significant along the plane of bending of the magnet (inplane in this case) rather than in the transverse plane.[23] Angular divergence ranging from 0.5 – 1.1° was added to match the inplane FWHM for all energies (table 3). Further simulations showed, however, that using an angular divergence to match the average of the inplane and crossplane R_{max} profile FWHM (i.e. using the same angular divergence inplane and crossplane) results in errors of less than 1% in clinical beam dose profiles.

III.C. Primary foil configuration

Measured and calculated R_{max} inplane profiles for the primary foil configuration are shown together in figure 7. The profiles for 9, 12, 15, 18 and 21 MeV electron beams have been normalized to 70, 60, 100, 90 and 80%, respectively. The 6 MeV electron beam does not utilize a primary scattering foil and is not included. Monte Carlo simulations and

measurements agreed to within 2.5% inplane and better than 2% for crossplane profiles. There was an apparent trend of increasing difference (between Monte Carlo and measurement) with increasing energy. A 0.2 – 0.3 (± 0.03) cm mismatch in the position of the inplane profile peaks was also evident. The peaks were defined by fitting Gaussian functions, restricted to the region of dose greater than 60% of maximum, and calculating the difference in the mean (μ). The beam angle was steered towards the position of the bremsstrahlung profile (R_x) peak (determined by fitting a Gaussian function to the profile restricted to region of profile out to ±10 cm from the collimator rotation axis for 6 – 9 MeV and ±5 cm for 12 – 21 MeV) as measured previously.[11] The R_x profile is dominated by bremsstrahlung x-rays from the exit window and primary scattering foil. Monte Carlo simulation showed that the fringe magnetic field had marginal effect on the offset of the x-ray fluence peak at isocenter, ranging from 0.15 cm at 6 MeV to 0.2 cm at 21 MeV. The beam angle would require adjustment outside the experimental uncertainties reported in section II.C.2 to improve the match to measurements. The fringe magnetic field was increased within the measurement uncertainty (17%) reducing the mismatch in the calculated and measured profile offsets by approximately 0.1 cm in the region of the profiles with greater than 50% of the maximum dose.

The offset of the jaws and multi-leaf collimator (MLC) from the collimator rotation axis was set in simulation based on the position of the field edge for the 18 MeV electron beam in primary foil configuration. This field is broad enough to be substantially collimated by the jaws and MLC and has a sharp field edge.[11] The positive and negative jaws were found to be offset by 0.01 cm and -0.01 cm, respectively, while the positive and negative MLC banks were offset by 0.03 cm and -0.02 cm, respectively.

Primary foil configuration was previously used to set the mean energy and Gaussian energy spread of the incident electron beams based on the measured percentage depth dose (PDD) curves.[11] As expected, the simulated fringe magnetic field was found to have

negligible effect on the nominal 6-21 MeV beam energy spectra at the phantom surface (as shown in figure 8 for the 21 MeV beam) and the central axis depth dose curves (not shown).

III.D. Clinical beam configuration

III.D.1. Sensitivity Analysis

The results of the sensitivity analysis of idealized symmetric beam R_{max} dose profiles to various sources of asymmetry are listed in table 1. Physical parameters varied were the lateral position of the secondary scattering foil and monitor chamber. These components were independently offset by 0.1 cm which represents a plausible physical offset.

The secondary foil offset has a significant effect on the flatness and symmetry of the beam. The effect is largest for the lowest energy beam (6 MeV) with effects on flatness and symmetry of 5.0% and 13.0%, respectively. The effects reduce with increasing energy and are 2-3 times lower at 21 MeV. The effect on the offset of the +50% and -50% dose points is minimal.

The most significant effect of a lateral shift of the monitor chamber is field offset (table 1). As stated in section II.A, with the jaws and MLC set to 40 × 40 cm^2, the monitor chamber collimates the beam and projects a 36 cm diameter field size at isocenter. The field offset is 0.35 cm at 6 MeV, increasing to 0.55 cm at 21 MeV. The effect is largest for the higher energy beams as electron scattering between the chamber and the measurement point is much less. Therefore it seems prudent to set the monitor chamber offset in simulations based on the position of the measured field edge for the higher energy beams (15 - 21 MeV).

The electron spot at the exit window (x_s) was laterally offset by the estimated experimental uncertainty in the measured spot position (0.05 cm). The spot position, similar to the monitor chamber, largely affects the field offset. The effect on flatness and symmetry is minimal and shows no trend with energy (table 1). The uncertainty in the measured spot

position could lead to 0.1 – 0.3 cm field offset for the 6 – 21 MeV beams, respectively. The lateral spot position is therefore a significant contributor to the field offset, along with the monitor chamber position.

The uncertainty in the beam angle increases with decreasing energy as outlined in section II.C.2, ranging from 0.52 – 0.09° for 6 – 21 MeV. This is carried through to the sensitivity analysis with the 6 MeV dose profile affected most by beam angle uncertainty (figure10 and table 1). The effect of the beam angle uncertainty on the higher energy (18 and 21 MeV) dose profiles is very small; less than 1% / 0.05 mm. This confirms that it is advisable to set the lateral offset of the monitor chamber using the high energy beam measurements since the uncertainty in the source parameters at the exit window are initially lower. The steps or "undulations" seen in the higher energy dose profiles (figure 9) are due to the 3 stepped layers of the Al secondary scattering foil. These undulation positions are also effective to set the lateral offset of the foil with the fringe magnetic field included in simulations.

The effects of the fringe magnetic field on the idealized symmetric dose profiles are shown graphically in figure 10 (and also quantified in table 1). The fringe field effects the flatness, symmetry, slope and (field) offset. The effect on flatness and symmetry is a maximum at 12 MeV. The effect on field offset is 0.3 cm (average). It is expected that the fringe field should have a similar effect for all energies since the measured fringe field was found to be a linear function of bending magnet current. However, there is some saturation of the bending magnet above 37 A[11] which could explain non-linear effects at higher energies. The fringe field is responsible for a single component of the measured inplane (y) offset which ranged from -0.71 to -1.99 cm. The remainder of the offset is the result of the spot offset and beam angle at the exit window, and the monitor chamber offset.

III.D.2. Comparison of measurements and simulations

Measured and Monte Carlo simulated dose profiles are compared in figure 11 for the 6 - 21 MeV clinical electron beams at 100 cm SSD. R_{max} crossplane (x) profiles have been normalized to 100% on the central axis. R_{max} inplane (y) profiles are normalized to 120% for clarity. Profiles in the bremsstrahlung (Rx) are also included, with the crossplane and inplane profiles normalized to 20% and 30%, respectively. The maximum differences between measured and simulated R_{max} dose profiles were 3%, 2.4%, 2.5%, 2.6%, 2.5% and 2% for 6 – 21 MeV, respectively, with comparison limited to the low dose gradient region (greater than 80% of maximum dose). The field edges matched to within 0.2 cm, 0.18 cm, 0.17 cm, 0.09 cm, 0.15 cm and 0.16 cm for 6 -21 MeV. There was an improved match (of up to 0.48 cm for 6 MeV) at the extreme edge of the field due to the simulation of the peripheral material below the MLC banks. Monte Carlo simulations show good agreement with the shape and offset of the measured R_x profiles in the bremsstahlung tail.

For clinical beam simulations, the source details, magnetic field and component offsets (now the same for all energies), were initially set as determined by experimental measurements. These parameters were then adjusted, iteratively and within respective experimental uncertainties and guided by sensitivity analysis, until a good match to measured profiles was achieved. With the secondary scattering foil and monitor chamber fixed in a single position for all energies, the simulated dose distributions are in better agreement with measurements than previous work.[10] The secondary scattering foil and monitor chamber lateral offsets from the collimator rotation axis were estimated from digital photographs and are listed in table 2. The offsets used in simulations are also given in table 2. The offsets were set to match the field edge and undulations of the measured dose profiles of the higher energy beams (18 and 21 MeV) with the fringe magnetic field included in simulations. Three out of four of the simulation offsets were within the uncertainty (0.03 cm) of those estimated by digital photographs. The simulation offsets were within 0.05 cm of those estimated from

digital photographs or a maximum of 0.02 cm outside the 0.03 cm photograph estimated uncertainty for all case.

Table 3 lists the energy – dependent source parameters used in clinical beam simulation. The asymmetric angular divergence was selected to match the FWHM of R_{max} dose profiles for exit window only configuration. The spot offsets and beam angles (direction cosines) were varied within experimental uncertainty (see section II.C.2) with the secondary foil and monitor chamber lateral position fixed and the fringe magnetic field simulated. This method resulted in a good match between measurements and simulations except for 6 MeV crossplane. With the 6 MeV crossplane spot offset within experimental uncertainty (spot placed at 0.0 cm), the monitor chamber would need to be offset by over 0.1 cm, outside the uncertainty of the photograph estimate and in the opposite direction to the offset which resulted in a good match to the field edge for the higher energies. Alternatively, the beam angle (or fringe magnetic field strength in the case of inplane disagreement) could also be adjusted (within uncertainty) to improve the match at the field edge, however, this also has a significant effect on the flatness and symmetry of the beam. It was therefore necessary to set the 6 MeV crossplane spot offset 0.06 cm outside the uncertainty of the measured spot position (Faddegon et al. 2009) with the monitor chamber lateral offset fixed for all energies (at 0.03 cm). Nevertheless, inclusion of the fringe magnetic field (as measured) and adjusting the beam angle, spot offset and secondary foil and monitor chamber offsets, realistically and within experimetal tolerances, has helped further restrict simulation parameters and resulted in excellent agreement with measured dose distributions.

IV. CONCLUSION

Large electron fields with the applicator removed and jaws and multi-leaf collimator set to maximum (40×40 cm^2) are most sensitive to electron source and treatment head simulation parameters. The fringe magnetic field from the bending magnet downstream of the exit

window is a significant contributor to beam asymmetry (up to 8%). Sensitivity analysis of profiles - with parameters varied within experimental uncertainty - is helpful in selecting simulation parameters. The magnetic field was measured and included in the simulation with the subsequent calculated dose showing a good match to measured electron beam dose distributions. There are many parameters which can be varied in order to obtain a good match between measured and simulated dose. With tightened tolerances on these parameters in this work, it is expected that the simulated fluence more accurately represents that of the actual linac.

ACKNOWLEDGEMENTS

We would like to thank James Lockhart (San Francisco State University) for the use of a Tesla-meter and discussion of magnetic field measurements.

REFERENCES

[1] Ma C-M, Ding M, Li J S, Lee M C, Pawlicki T and Deng J 2003 A comparative dosimetric study on tangential photon beams, intensity-modulated radiation therapy (IMRT) and modulated electron radiotherapy (MERT) for breast cancer treatment Phys. Med. Biol. 48 909

[2] Ge Y, O'Shea T and Faddegon B 2010 X-Ray Plus Electron Radiotherapy with An Extendable MLC Med. Phys. 37 3375

[3] Jiang S B, Kapur A and Ma C-M 2000 Electron beam modeling and commissioning for Monte Carlo treatment planning Med. Phys. 27 180

[4] Hu Y A, Song H, Chen Z, Zhou S and Yin F-F 2008 Evaluation of an electron Monte Carlo dose calculation algorithm for electron beams Journal Appl. Clin. Med. Phys. 9 (3) 1

[5] Fix M K, Frei D, Volken W, Neuenschwander H, Born E J and Manser P 2010 Monte Carlo dose calculation improvements for low energy electron beams using eMC Phys. Med. Biol. 55 4577

[6] Huang V W, Seuntjens J, Devic S and Verhaegen F 2005 Experimental determination of electron source parameters for accurate Monte Carlo calculation of large field electron therapy Phys. Med. Biol. 50 779-786

[7] Weinberg R, Antolak J A, Starkschall G, Kudchadker R J, White R A and Hogstrom K R 2009 Influence of source parameters on large-field electron beam profiles calculated using Monte Carlo methods Phys. Med. Biol. 54 105-116

[8] Björk P, Knöös T and Nilsson P 2002 Influence of initial electron beam characteristics on Monte Carlo calculated absorbed dose distributions for linear accelerator electron beams Phys. Med. Biol. 47 4019-4041

[9] Faddegon B A, Schreiber E and Ding X 2005 Monte Carlo simulation of large electron fields Phys. Med. Biol. 50 741

[10] Faddegon B A, Perl J and Asai M 2008 Monte Carlo simulation of large electron fields Phys. Med. Biol. 53 1497-1510

[11] Faddegon B A, Sawkey D L, O'Shea T P, McEwen M and Ross C 2009 Treatment head disassembly to improve the accuracy of large electron field simulation Med. Phys. 36 (10) 4577-91

[12] O'Shea T P, Sawkey D L, Foley M J and Faddegon B A 2010 Monte Carlo commissioning of clinical electron beams using large field measurements Phys. Med. Biol. 55 4083

[13] Oline L, Krispel F and Sagalovsky L 1990 Simulation of Magnetic Optics in the Focusing Magnet of a Medical Accelerator 2nd European Particle Accelerator Conference (EPAC 90) Proceedings 1807

[14] Kawrakow I and Rogers D W O 2006 The EGSnrc code system: monte carlo simulation of electron and photon transport NRCC Report PIRS-701

[15] Rogers D W O, Faddegon B A, Ding G X, Ma C M and We J 1995 BEAM: A Monte Carlo code to simulate radiotherapy treatment units Med. Phys. 22 (5) 503-524

[16] Faddegon B A, Balogh J, Mackenzie R and Scora D 1998 Clinical considerations of Monte Carlo for electron radiotherapy treatment planning Radiation Physics and Chemistry 53 217-227

[17] Sawkey D L and Faddegon B A 2009 Determination of electron energy, spectral width, and beam divergence at the exit window for clinical megavoltage x-ray beams Med. Phys. 36 698

[18] Schreiber E C and Faddegon B A 2005 Sensitivity of large-field electron beams to variations in a Monte Carlo accelerator model Phys. Med. Biol. 50 769

[19] Bieljew A F 1993 The effect of strong longitudinal magnetic fields on dose deposition from electron and photon beams Med. Phys. 20 (4) 1171

[20] Lee M C and Ma C-M 2000 Monte Carlo characterization of clinical electron beams in transverse magnetic fields Phys. Med. Biol. 45 (10) 2947

[21] Li Z A, Naqvi S, Chu J and Reiffel L 2001 Conformal photon-beam therapy with transverse magnetic fields: A Monte Carlo study Med. Phys. 28 127

[22] Kirkby C, Stanescu T, Rathee S, Carlone M, Murray B and Fallone B G 2008 Patient dosimetry for hybrid MRI-radiotherapy systems Med. Phys. 35 (3) 1019

[23] Karzmark C J, Nunan C S and Tanabe E 1993 Medical Electron Accelerators McGraw-Hill ISBN-13: 978-0071054102

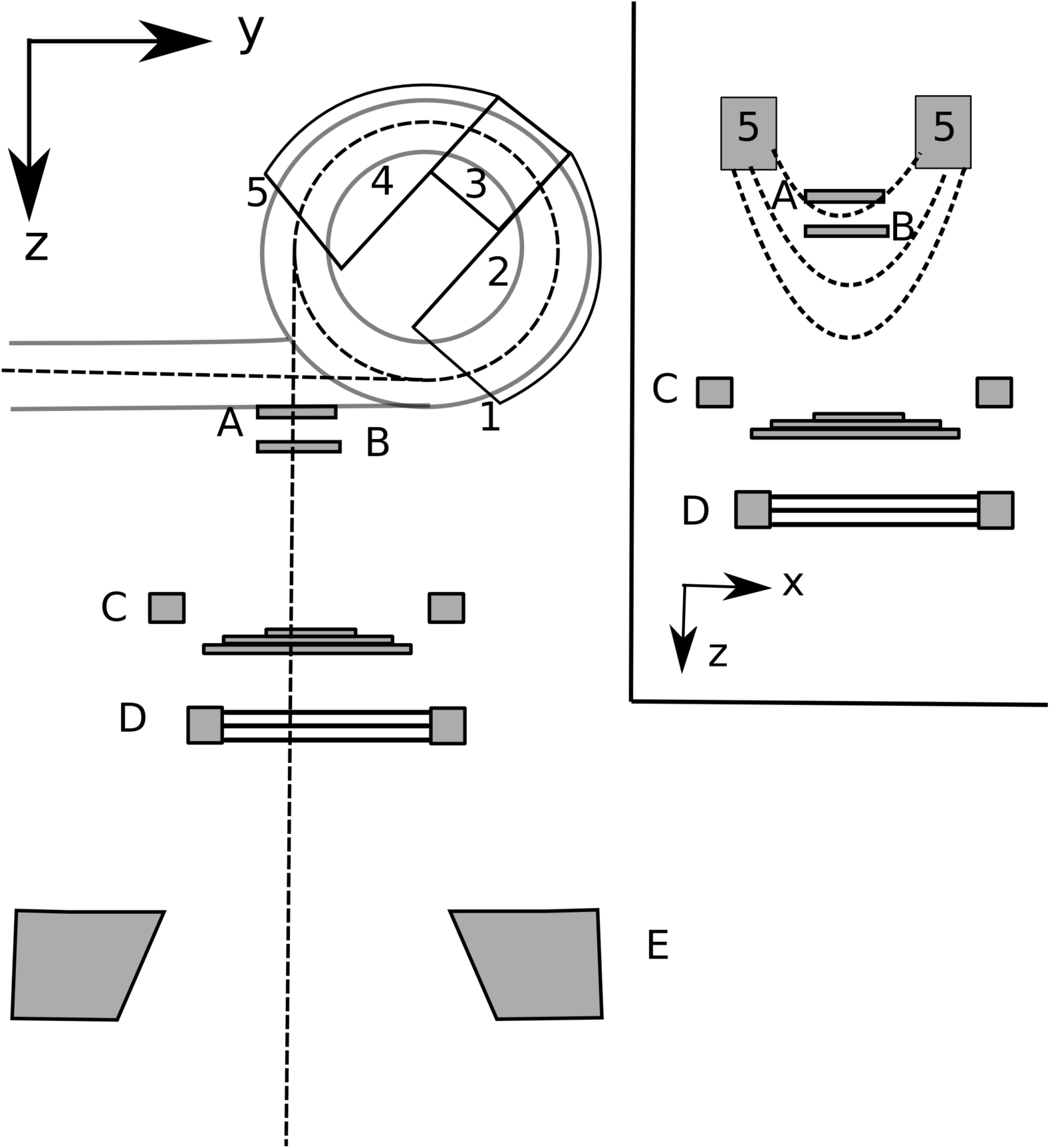
y
z
5
4
3
2
1
A
B
C
D
E
5
5
A
B
C
D
x
z

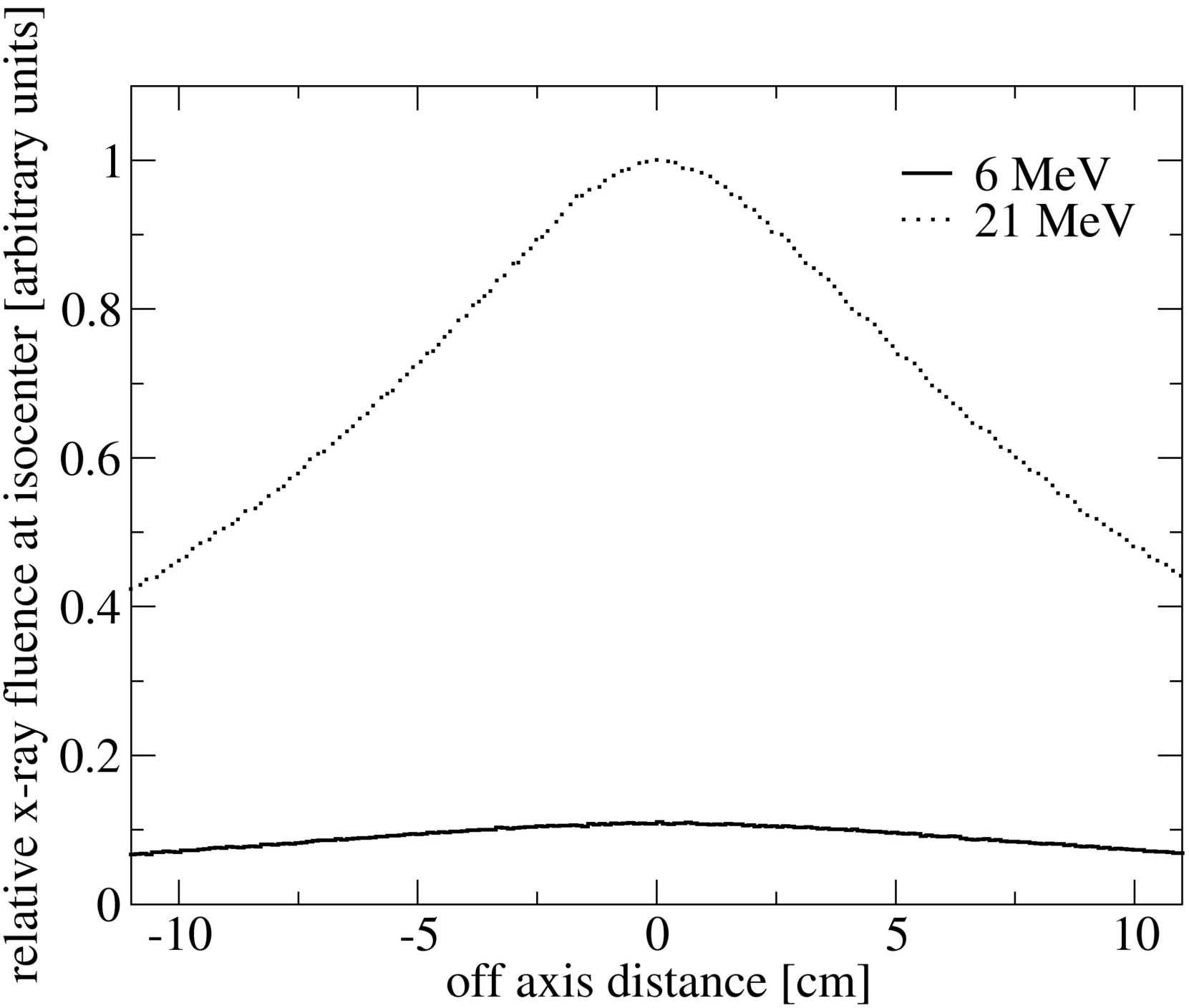
relative x-ray fluence at isocenter [arbitrary units]
1
0.8
0.6
0.4
0.2
0
-10
-5
0
5
10
off axis distance [cm]
6 MeV
21 MeV

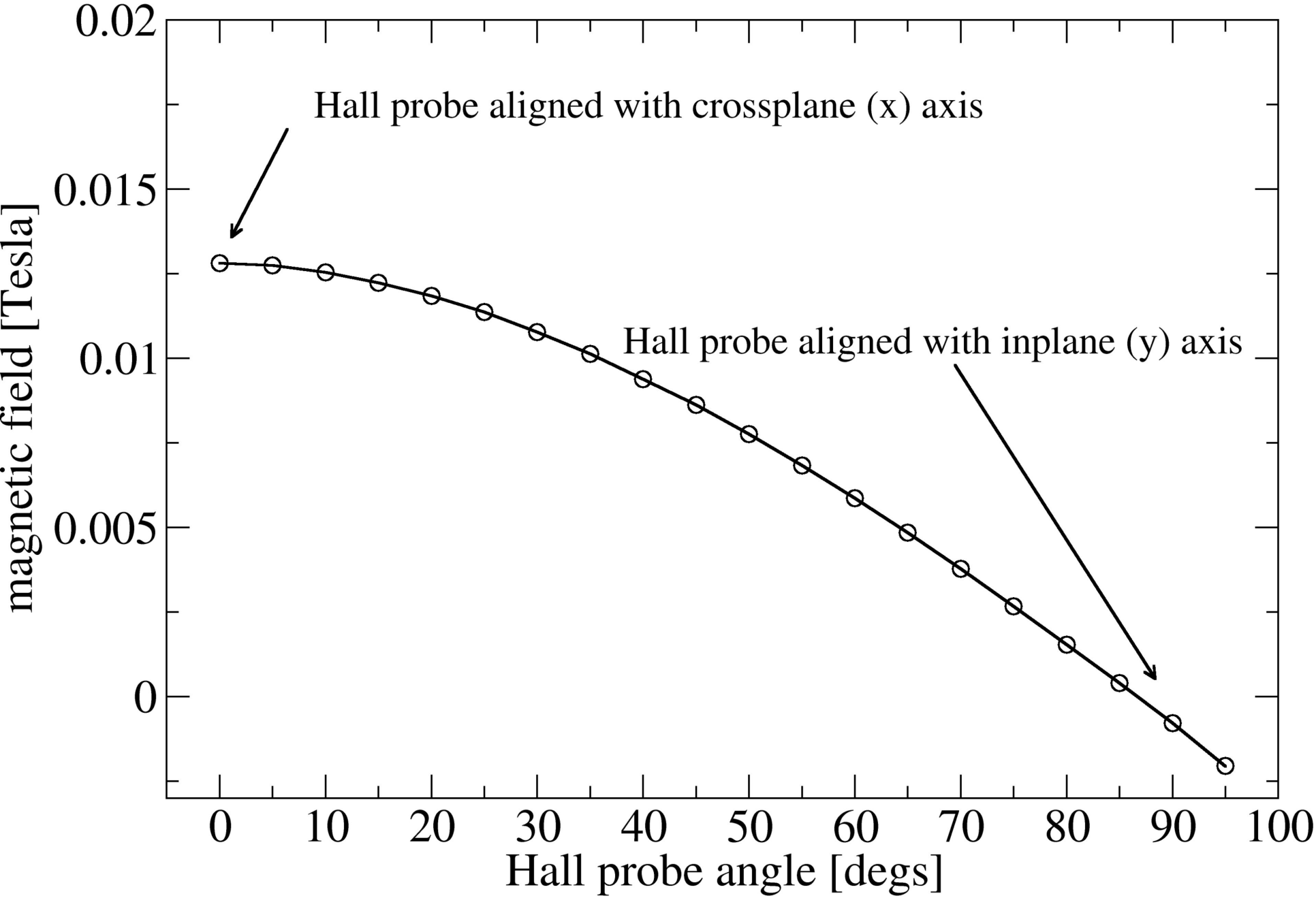
0.02
0.015
0.01
0.005
0
magnetic field [Tesla]
Hall probe aligned with crossplane (x) axis
Hall probe aligned with inplane (y) axis
0
10
20
30
40
50
60
70
80
90
100
Hall probe angle [degs]

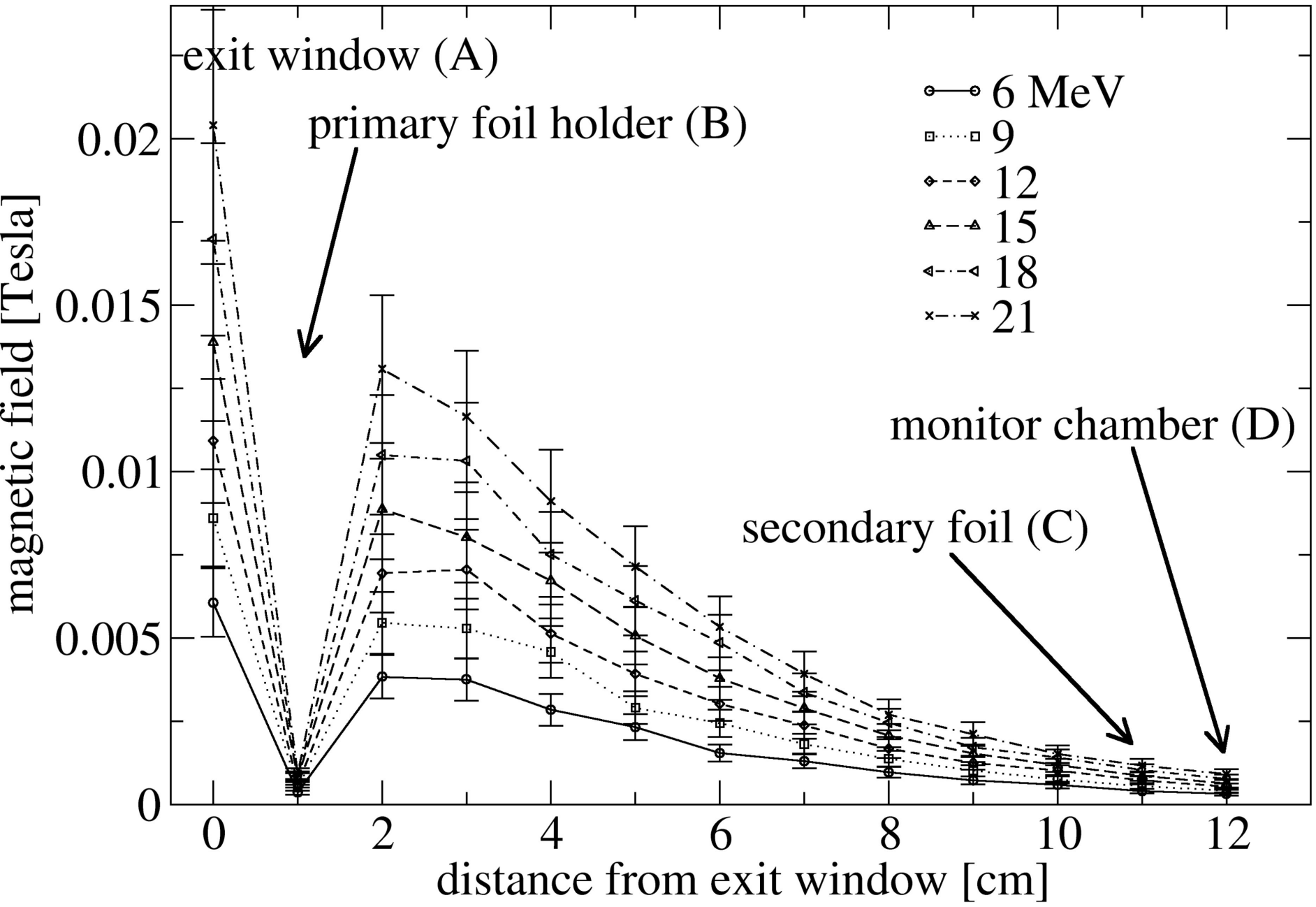
exit window (A)
primary foil holder (B)
secondary foil (C)
monitor chamber (D)
6 MeV
9
12
15
18
21
magnetic field [Tesla]
0
0.005
0.01
0.015
0.02
0
2
4
6
8
10
12
distance from exit window [cm]

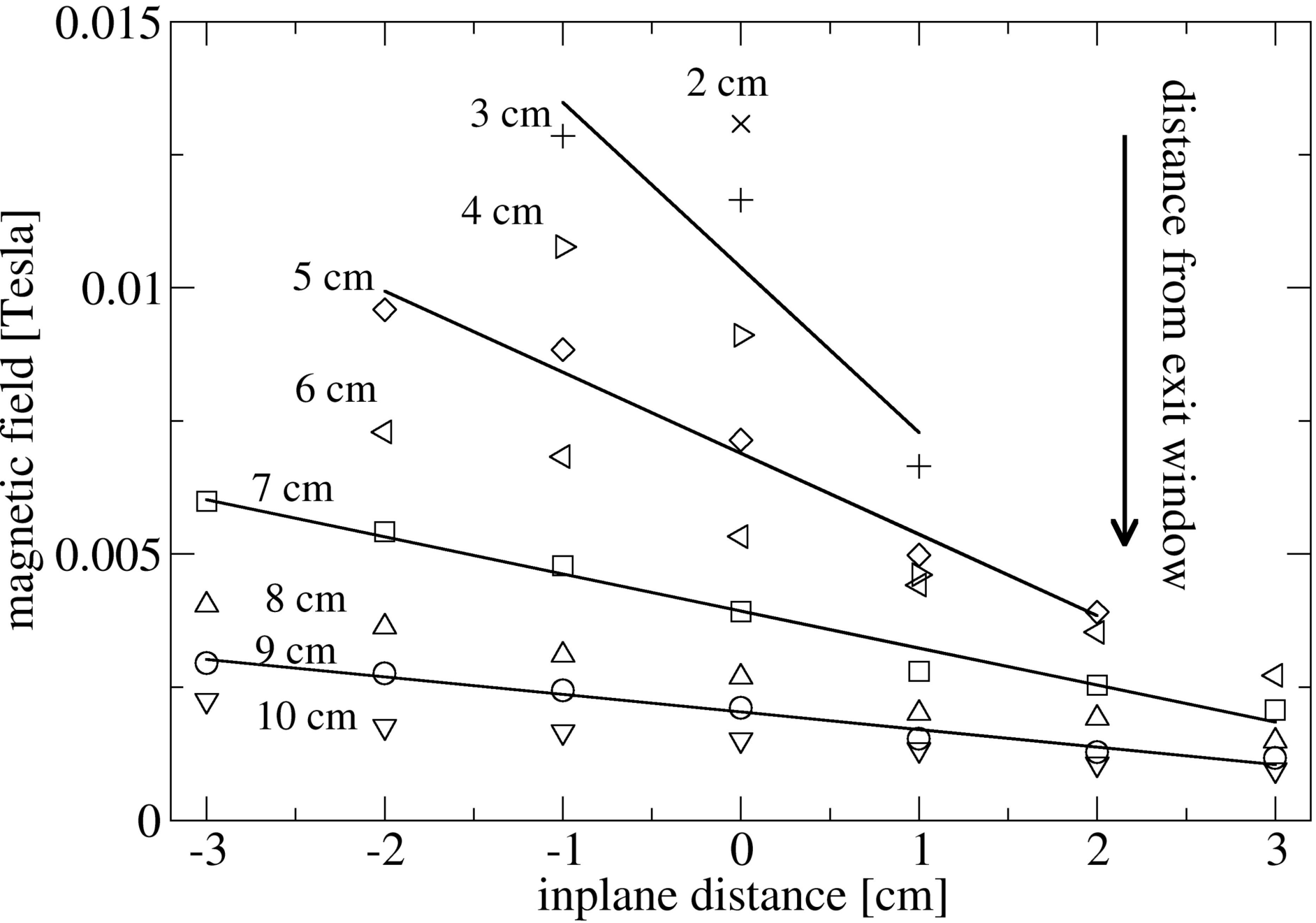
0.015
0.01
0.005
0
magnetic field [Tesla]
-3
-2
-1
0
1
2
3
inplane distance [cm]
2 cm
3 cm
4 cm
5 cm
6 cm
7 cm
8 cm
9 cm
10 cm
distance from exit window

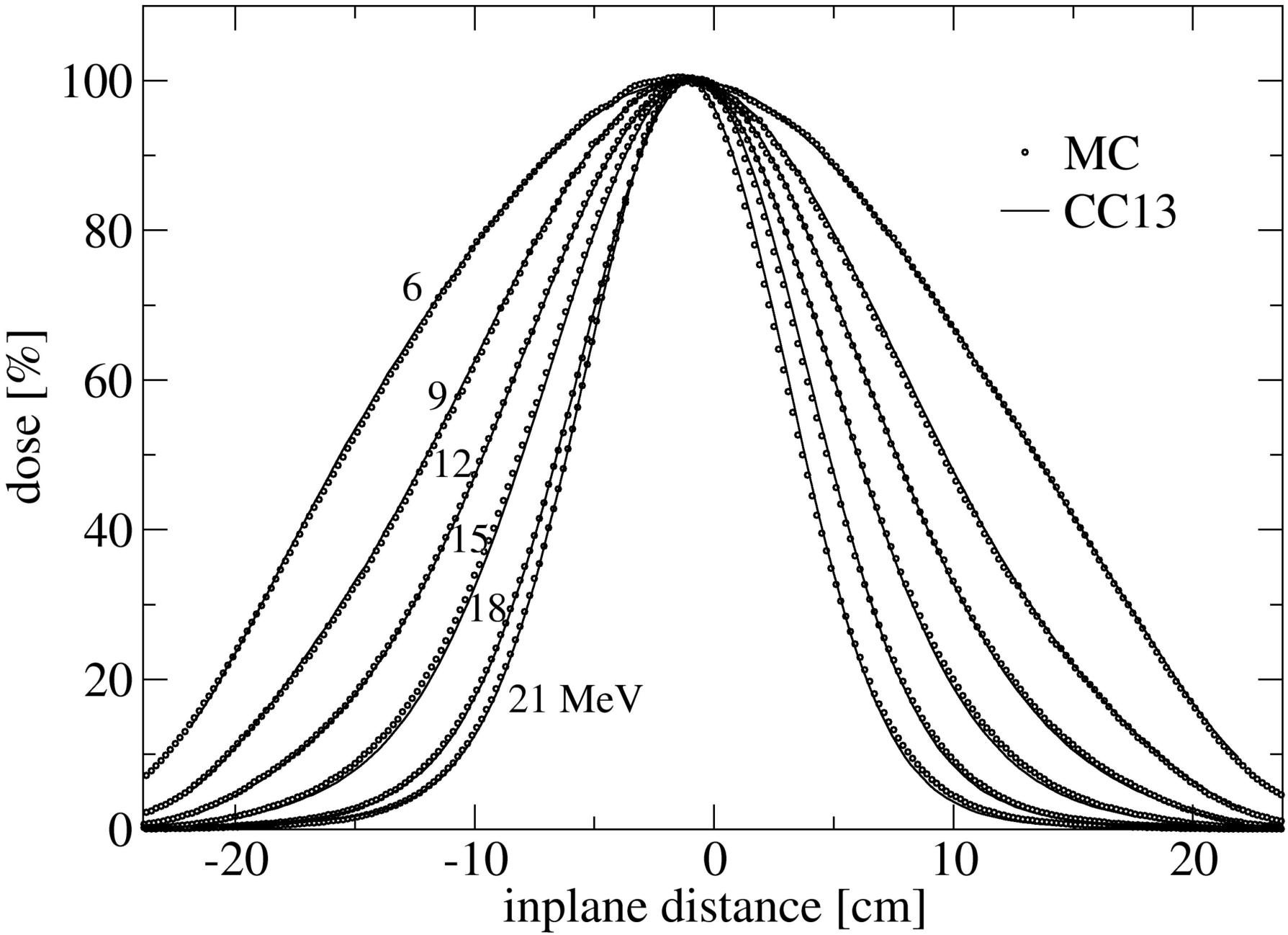
100
80
60
40
20
0
dose [%]
-20
-10
0
10
20
inplane distance [cm]
MC
CC13
6
9
12
15
18
21 MeV

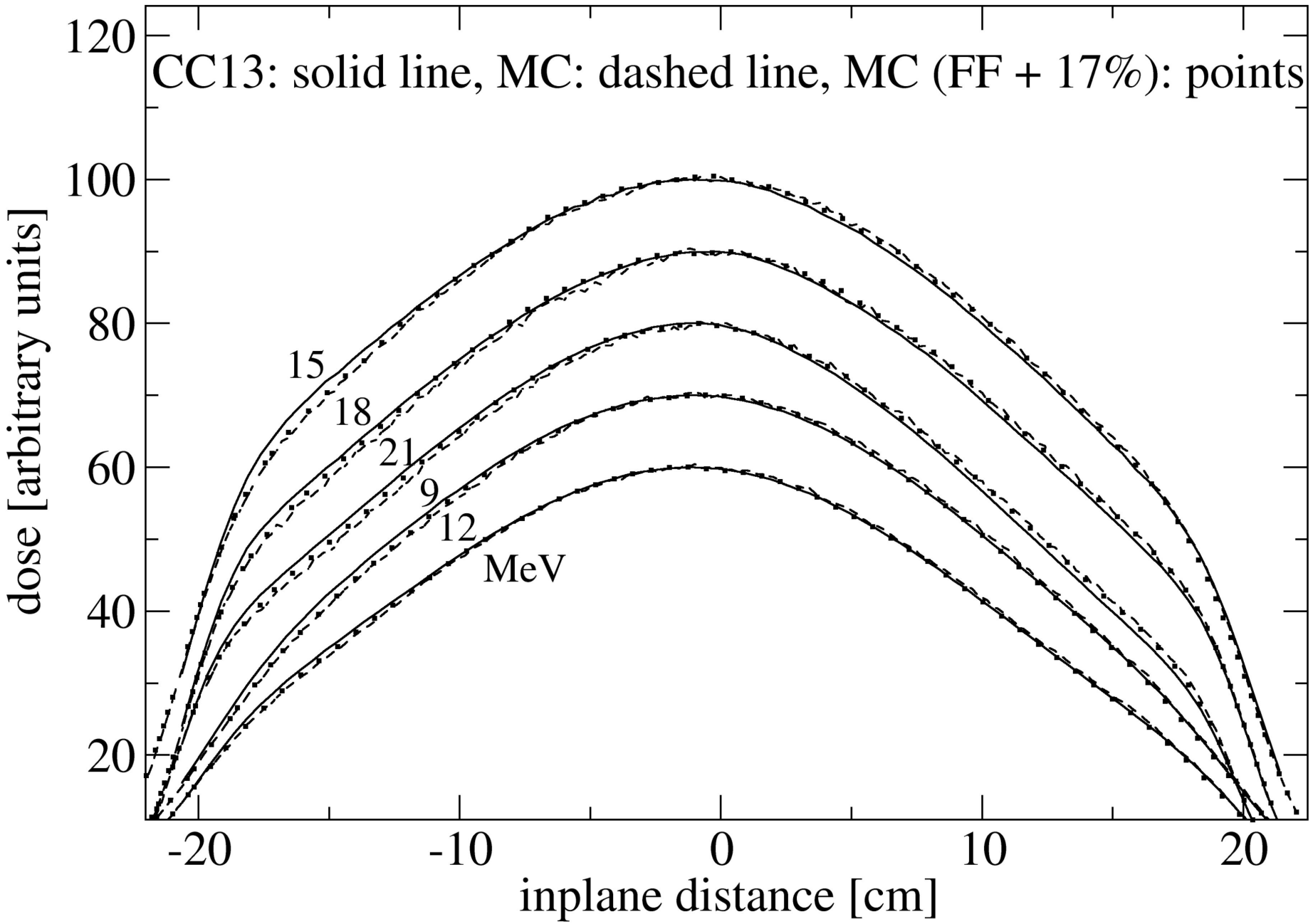
CC13: solid line, MC: dashed line, MC (FF + 17%): points
dose [arbitrary units]
inplane distance [cm]
120
100
80
60
40
20
-20
-10
0
10
20
15
18
21
9
12
MeV

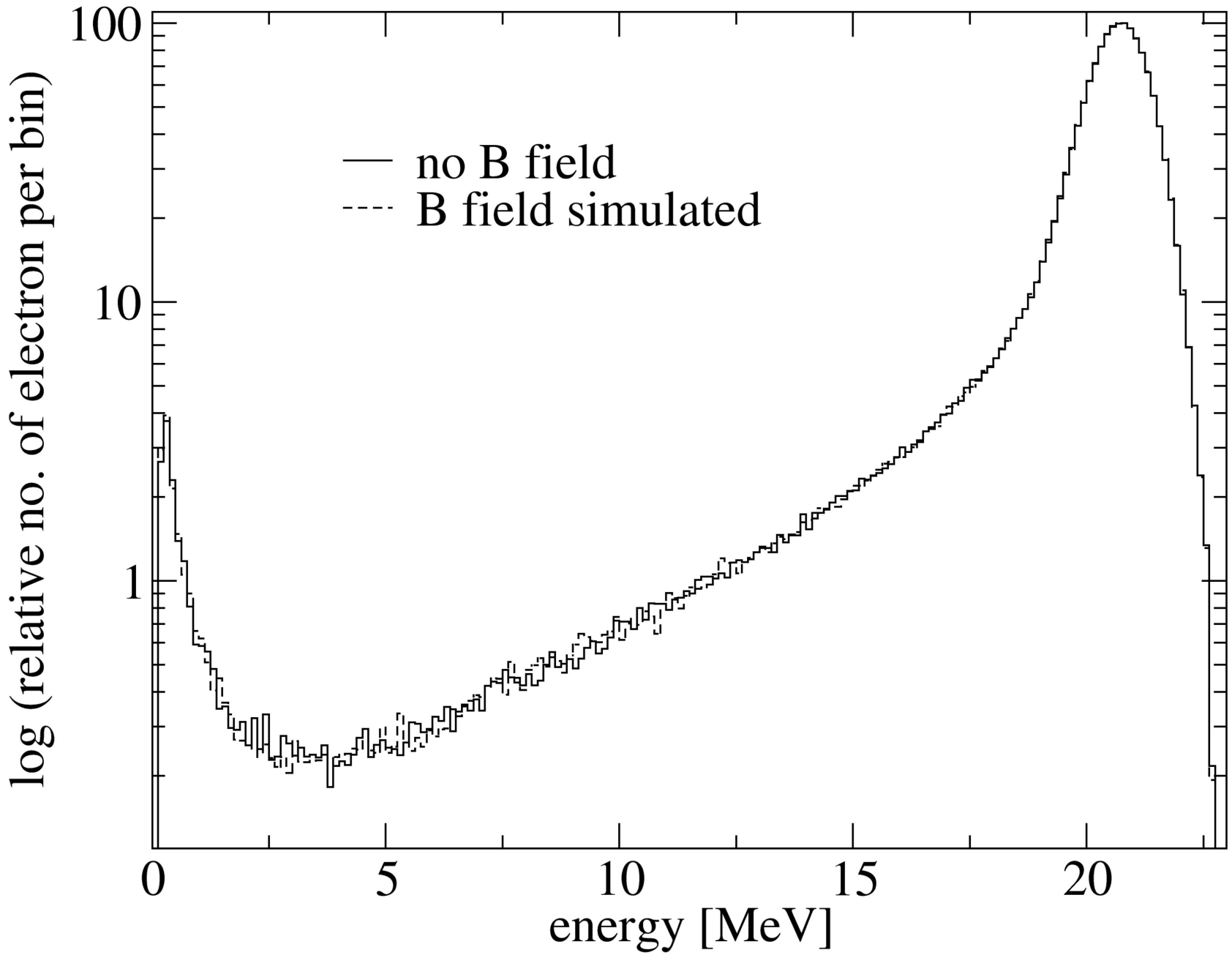
100
10
1
log (relative no. of electron per bin)
no B field
B field simulated
0
5
10
15
20
energy [MeV]

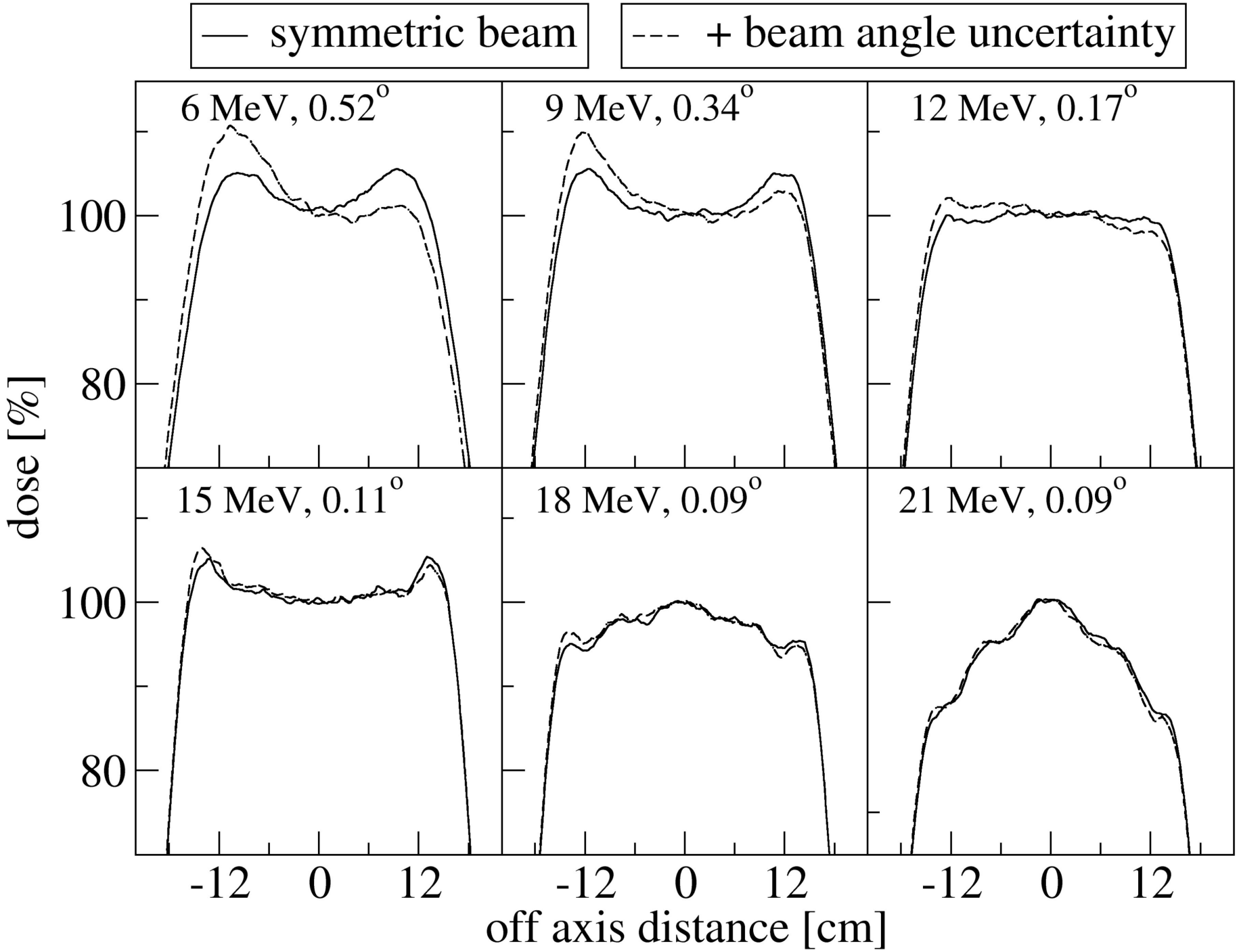
— symmetric beam
--- + beam angle uncertainty
6 MeV, 0.52°
9 MeV, 0.34°
12 MeV, 0.17°
15 MeV, 0.11°
18 MeV, 0.09°
21 MeV, 0.09°
100
80
100
80
dose [%]
-12
0
12
-12
0
12
-12
0
12
off axis distance [cm]

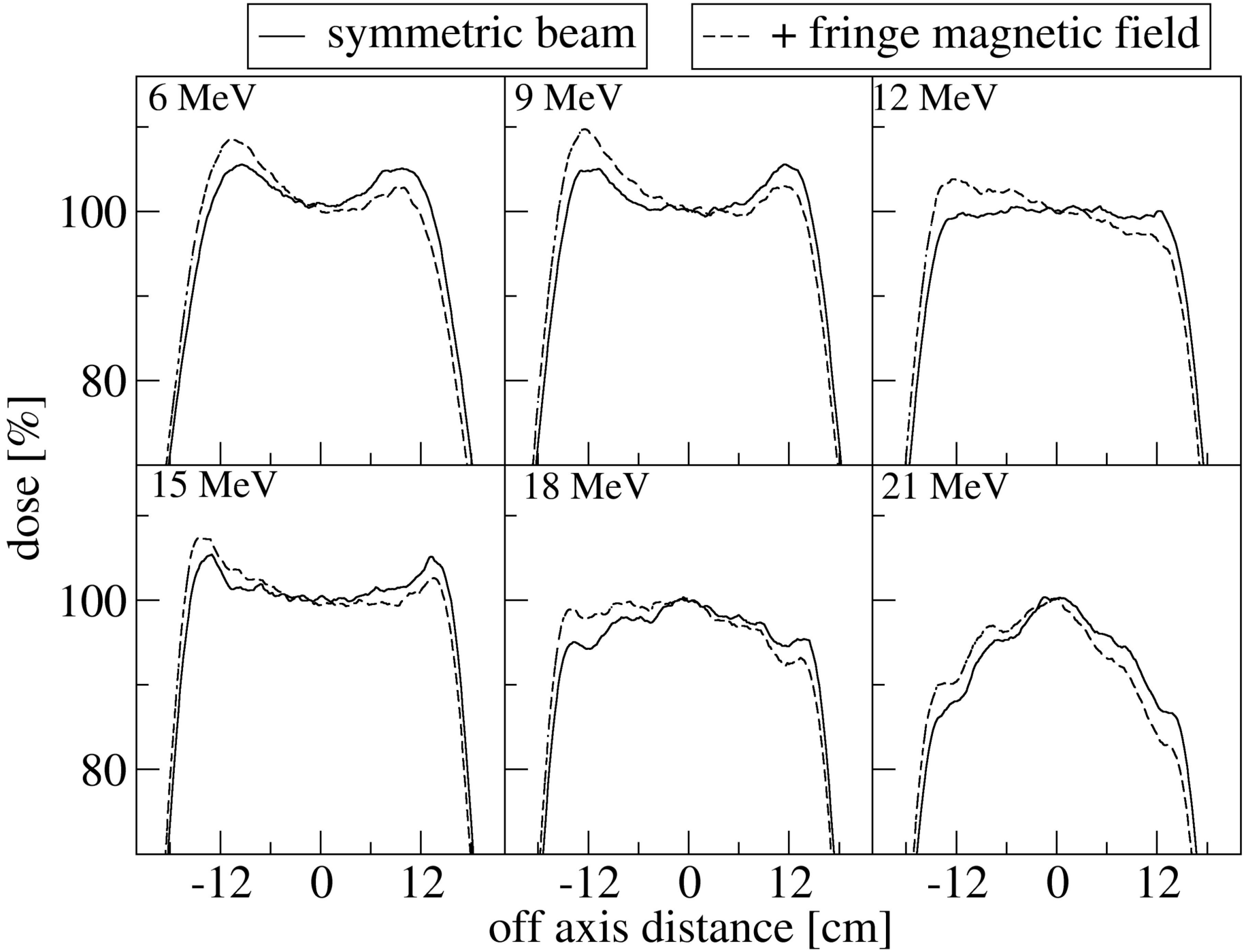
— symmetric beam
--- + fringe magnetic field
6 MeV
9 MeV
12 MeV
15 MeV
18 MeV
21 MeV
100
80
100
80
dose [%]
-12
0
12
-12
0
12
-12
0
12
off axis distance [cm]

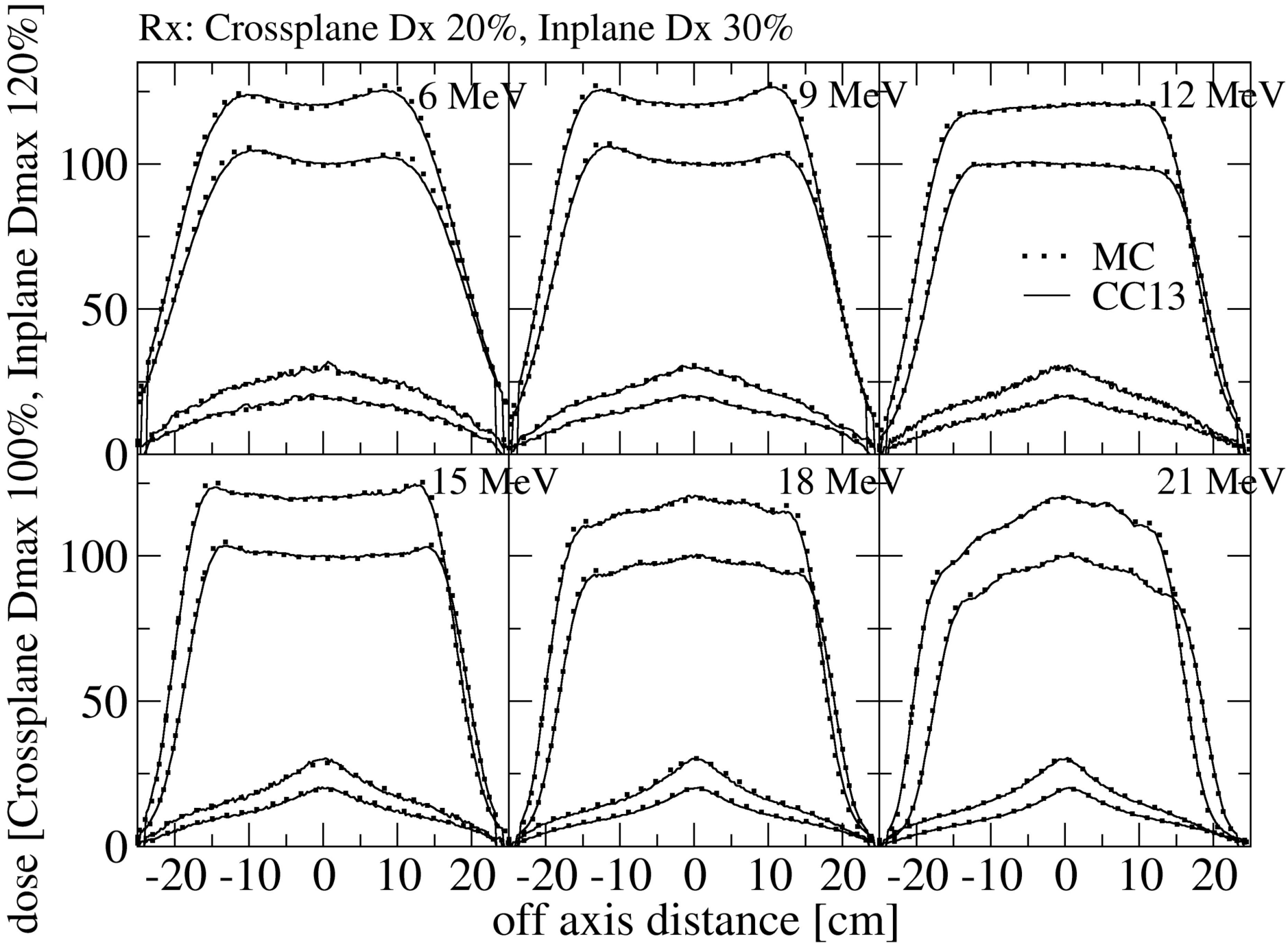
Rx: Crossplane Dx 20%, Inplane Dx 30%
6 MeV
9 MeV
12 MeV
15 MeV
18 MeV
21 MeV
MC
CC13
dose [Crossplane Dmax 100%, Inplane Dmax 120%]
off axis distance [cm]
0
50
100
-20 -10 0 10 20

Table 1. Effect of various sources of asymmetry on initial idealized 6 – 21 MeV symmetric electron beam. The experimetal uncertainy in the spot offset was 0.05 cm. The experimetal uncertainties in the beam angle (directional cosines) were 0.009, 0.006, 0.003, 0.002, 0.0015 and 0.0015 for 6 – 21 MeV, respectively. The initial symmetric beam had flatness ($Flat_{baseline}$) of 2.4%, 3.0% 0.35%, 1.7%, 2.8% and 6.65% for 6 – 21 MeV, respectively. The slope (of the line through the points at 12 cm and -12 cm from the central axis) is quoted to the nearest 0.05 % / cm and field offset to the nearest 0.05 cm.

Assymetry	**Energy [MeV]**	$\Delta_{\textbf{Flatness}}$ **[%]**	**Symmetry [%]**	**Slope [% / cm]**	**Field offset [cm]**
Sec. Foil offset	6	5.0	13.0	0.5	0.1
[0.1 cm]	9	3.6	14.2	0.6	0.05
	12	5.7	12.5	0.5	0.0
	15	3.4	10.5	0.4	0.0
	18	2.0	8.1	0.3	0.0
	21	1.8	7.2	0.3	0.15
Mon. offset	6	1.0	6.0	0.25	0.35
[0.1 cm]	9	0.3	4.7	0.2	0.45
	12	1.0	3.2	0.1	0.45
	15	0.1	0.4	0.0	0.55
	18	0.6	1.5	0.1	0.50
	21	0.0	0.4	0.0	0.55
Spot offset	6	0.1	3.6	0.15	0.1
[exp. uncert.]	9	0.75	3.4	0.1	0.25
	12	1.9	4.0	0.2	0.25
	15	0.9	4.9	0.2	0.3
	18	1.1	3.8	0.2	0.2
	21	1.0	3.6	0.15	0.3
Beam angle	6	3.1	9.2	0.4	0.3
[exp. uncert.]	9	1.75	7.8	0.3	0.15
	12	1.6	4.4	0.1	0.05
	15	0.5	2.0	0.1	0.05
	18	0.6	1.0	0.05	0.0
	21	0.5	0.9	0.05	0.0

Fringe B field	6	1.7	7.5	0.3	0.3
[measured]	9	1.7	7.3	0.3	0.35
	12	3.2	7.6	0.3	0.35
	15	1.0	3.5	0.15	0.3
	18	1.2	5.8	0.2	0.25
	21	2.0	5.8	0.2	0.3

Table 2. Offset of secondary scattering foil and electron monitor chamber from collimator rotation axis.

	Secondary Scat. foil		**Monitor chamber**	
	Digital photo.	*Simulation*	*Digital photo.*	*Simulation*
Crossplane [cm]	-0.01 ± 0.03	0.02	0.07 ± 0.03	0.03
Inplane [cm]	-0.04 ± 0.03	-0.065	-0.05 ± 0.03	-0.10

Table 3. Energy – dependent source parameters at the exit window used for clinical treatment head simulations. Spot position is relative to the collimator rotation axis. Root mean square angular divergence.

Energy [MeV]		**6**	**9**	**12**	**15**	**18**	**21**
Spot Offset (x_s) [cm]	**Crossplane**	0.06	0.02	0.01	-0.02	-0.01	-0.02
	Inplane	0.05	0.02	0.07	0.02	0.04	0.18
Direction cosine (Θ)	**Crossplane**	-0.006	-0.0035	0.0	0.002	0.003	0.005
	Inplane	-0.001	0.0	-0.003	0.0	0.002	-0.004
Angular Div. $\phi'(\Theta)$ [°]	**Crossplane**	-	0.4	0.6	0.85	0.6	0.2
	Inplane	0.7	0.8	0.85	1.1	0.8	0.5

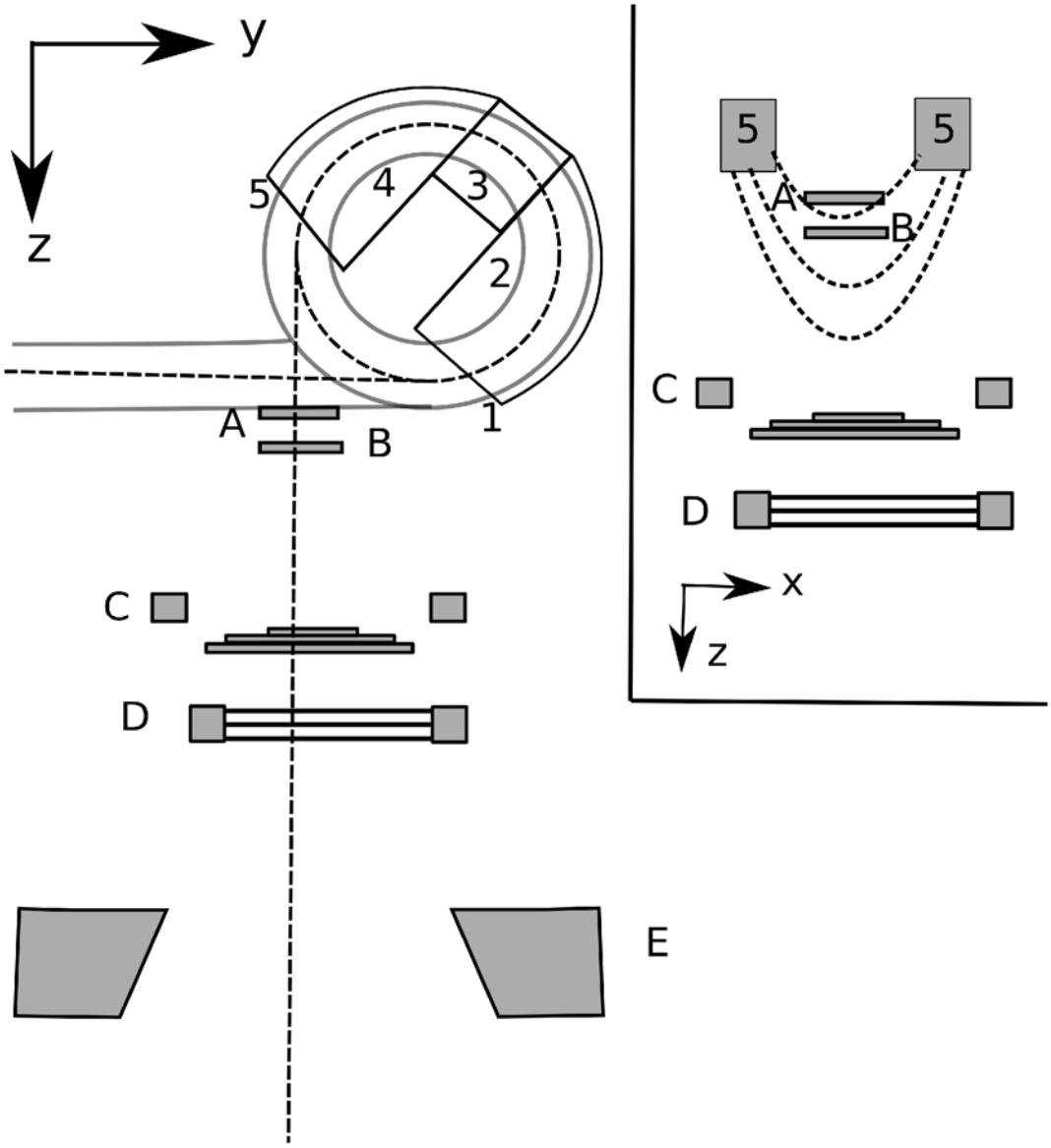

Figure 1. Diagram of Siemens Oncor 270° bending magnet and electron treatment head. The bending magnet is composed of 5 distinct regions: (1) entrance pole face edge, (2) constant field region, (3) focusing gradient region. (4) constant field region and (5) exit pole face edge. The exit pole face is angled and has an extended fringe field to focus the beam. The key components of the treatment head modelled in BEAMnrc are also shown in this diagram: the exit window (A), primary scattering foil (B), secondary scattering foil (C), electron monitor chamber (D) and secondary collimators (E). The inset figure demonstrates how the fringe field extends below the exit window modifying the electron beam characteristics after it has exited the envelope.

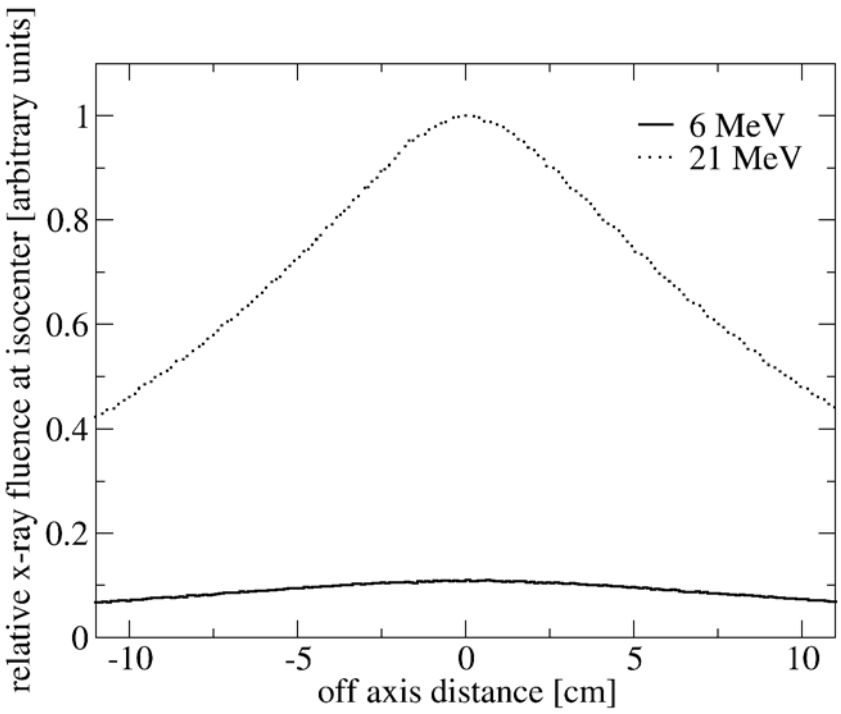

Figure 2. Bremsstrahlung fluence for 6 and 21 MeV electron beams normalized to the peak of the 21 MeV profile to hightlight the relatively flat 6 MeV profile which leads to a larger uncertainty in the beam angle at the exit window.

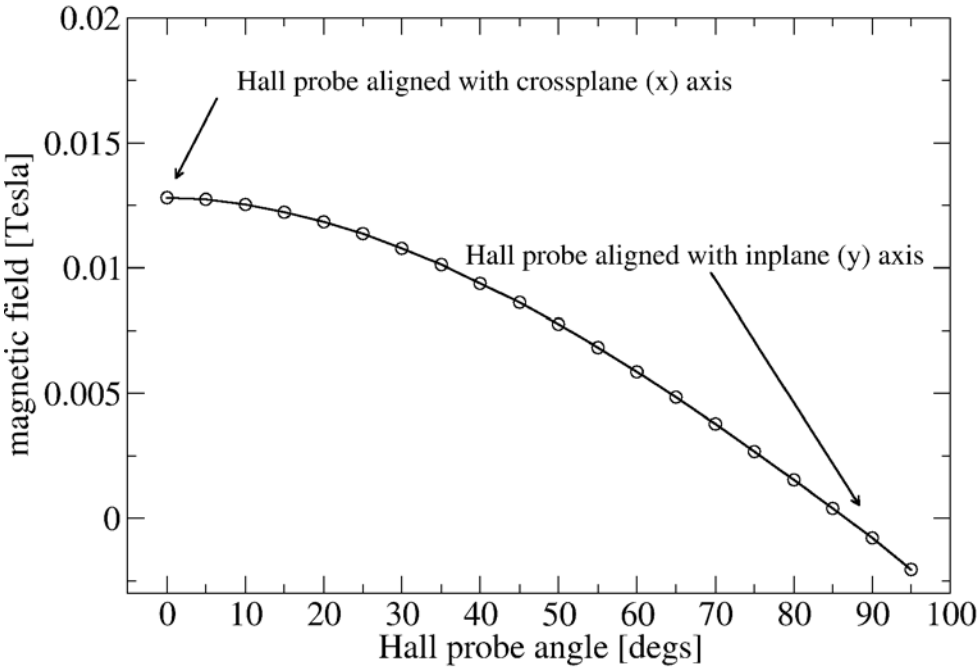

Figure 3. Fringe magnetic field measured for 21 MeV at 2 cm from the exit window with the hall probe flat fixed to the collimator which was then rotated through 90°. The probe is orientated perpendicular to the gun (crossplane) at an angle of 0° (max. magnetic field). Earth's magnetic field is 50×10^{-6} T and has a negligible effect on the electron beam deflection at isocenter.

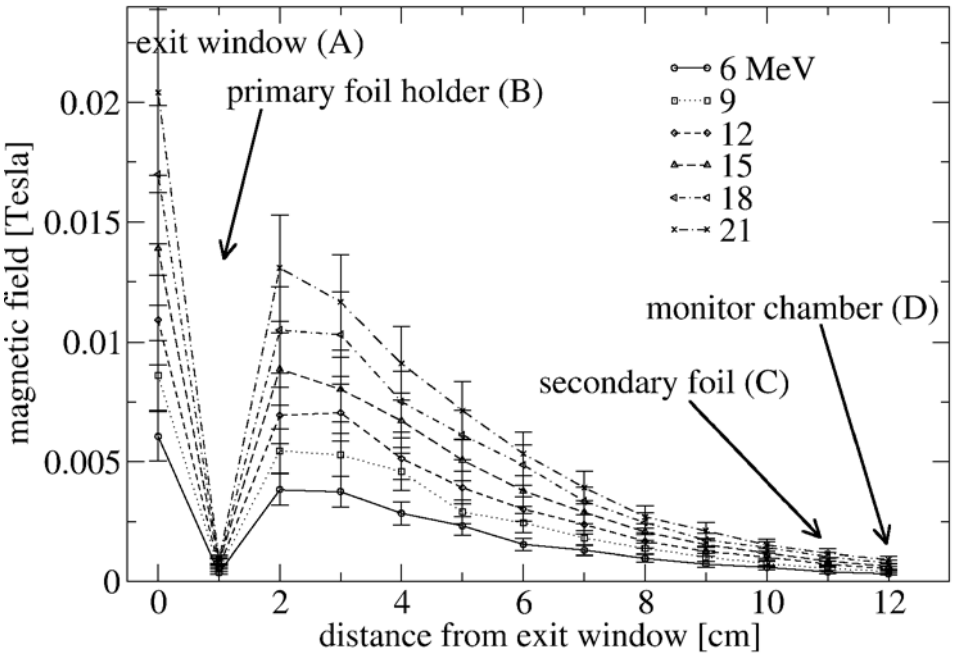

Figure 4. Variation in fringe magnetic field with distance from the exit window for nominal 6 – 21 MeV electron beams (bending magnet current: 13.1 – 42.2 A). The field is a maximum at the exit window dropping to ~5% at the secondary foil. The approximate positions of the exit window, primary foil holder, secondary foil and monitor chamber are indicated.

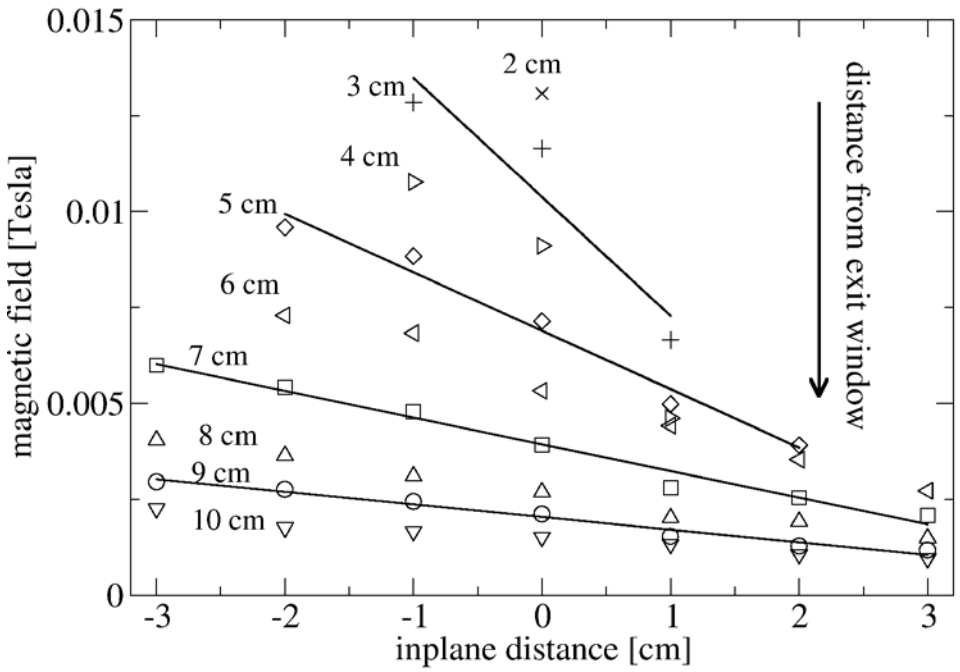

Figure 5. Fringe magnetic field measured across the inplane (y) axis (with distance from the collimator rotation axis) for the 21 MeV beam (42.2 A) and at 2 – 10 cm from the exit window. The magnetic field is up to 3 times higher on the negative inplane side. Linear regression was performed on the data at 3, 5, 7 and 9 cm from the exit window to highlight the field gradient.

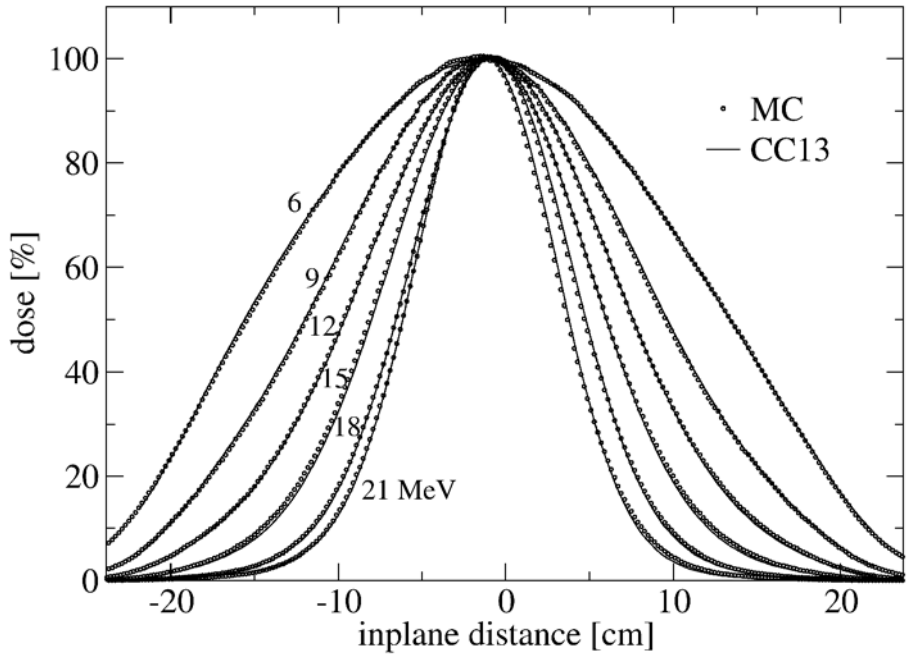

Figure 6. Comparison of CC13 and Monte Carlo simulated inplane dose profiles with exit window only in the beam. The exit window water channel was thickened to match the 6 MeV crossplane FWHM with RMS angular divergence added to match the broader inplane profiles and for higher energies (table 3).

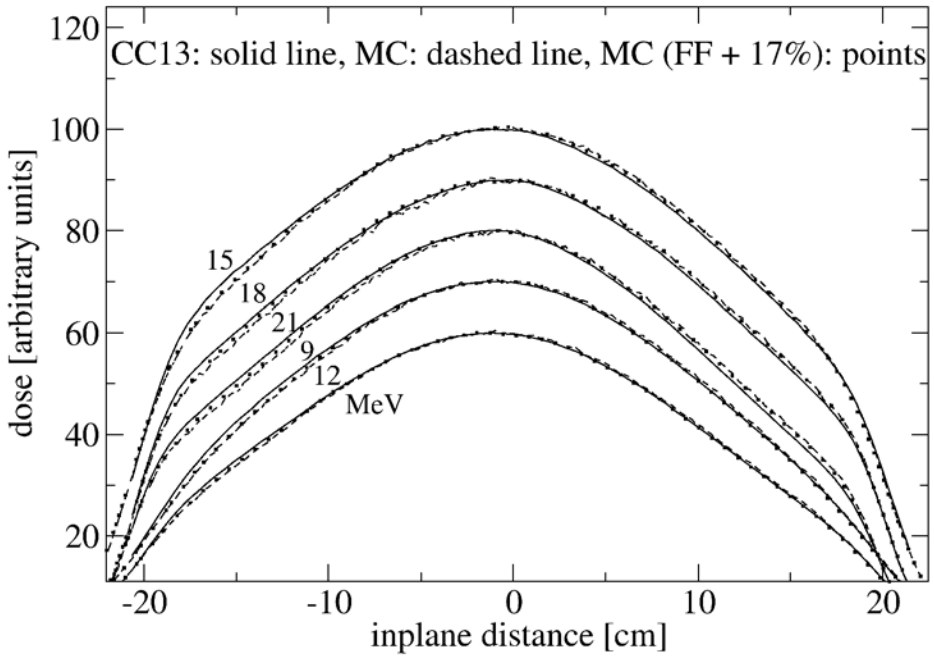

Figure 7. Comparison of CC13 and Monte Carlo simulated inplane dose profiles with the primary foil in the beam. Monte Carlo calculations are shown with the measured fringe magnetic field (dashed lines) and measured magnetic field increased by 17% (the total experimental uncertainty in the measurement, points) included in simulations. Primary foil simulations used the same source details as the exit window only configuration.

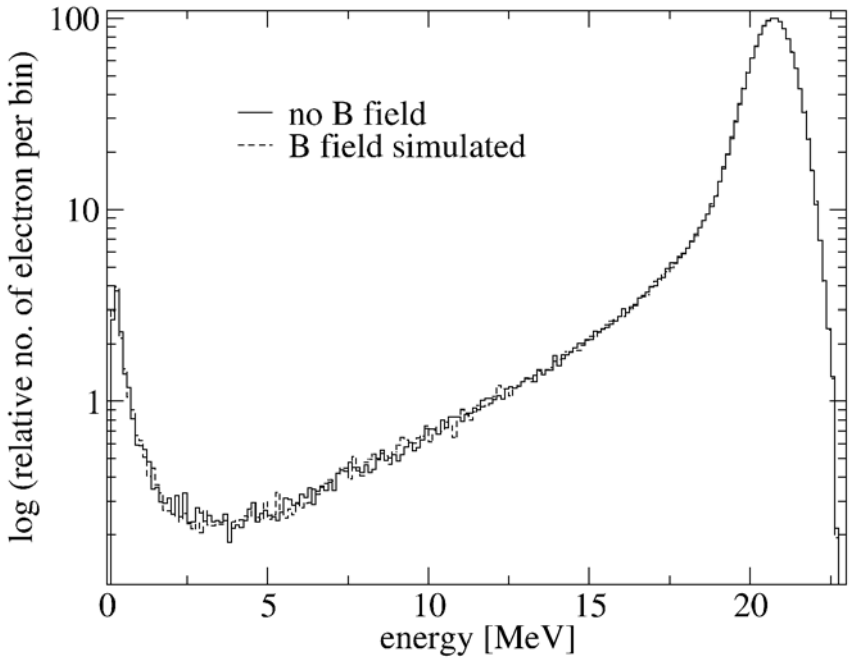

Figure 8. Energy spectral distribution on a 12×12 cm^2 plane at 100 cm SSD for 21 MeV electron beam. The simulated fringe magnetic field has negligible effect on the distribution and spectral peak. Note the vertical axis is logarithmic.

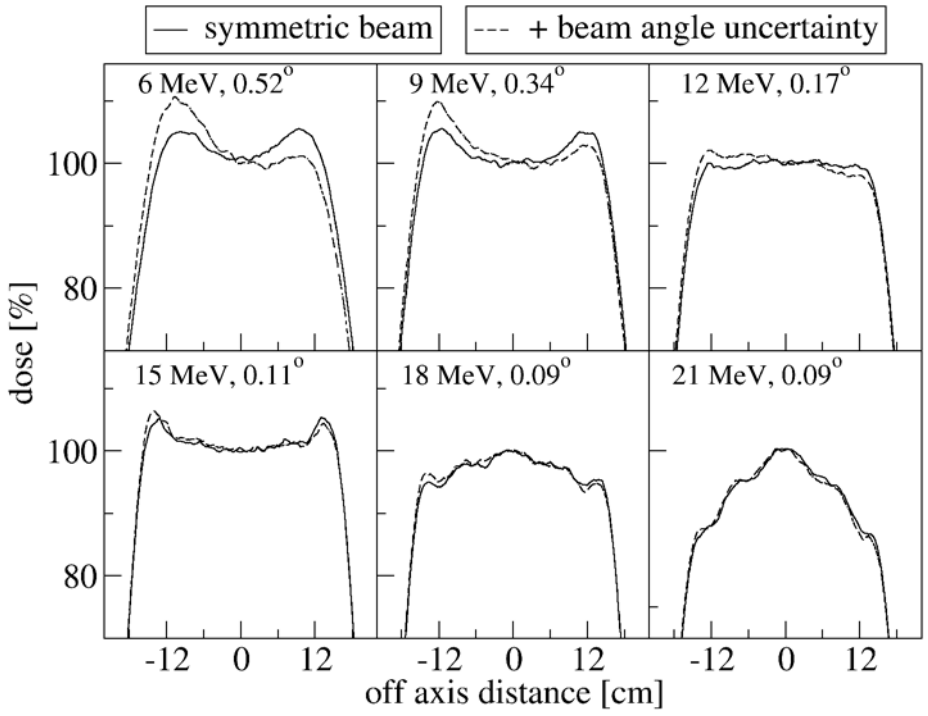

Figure 9. The effect of beam angle - varied by experimental uncertainty – on symmetric dose profiles (which contain no sources of asymmetry) for 6 – 21 MeV beams and 40×40 cm^2 field size. Effects are quantified in table 1.

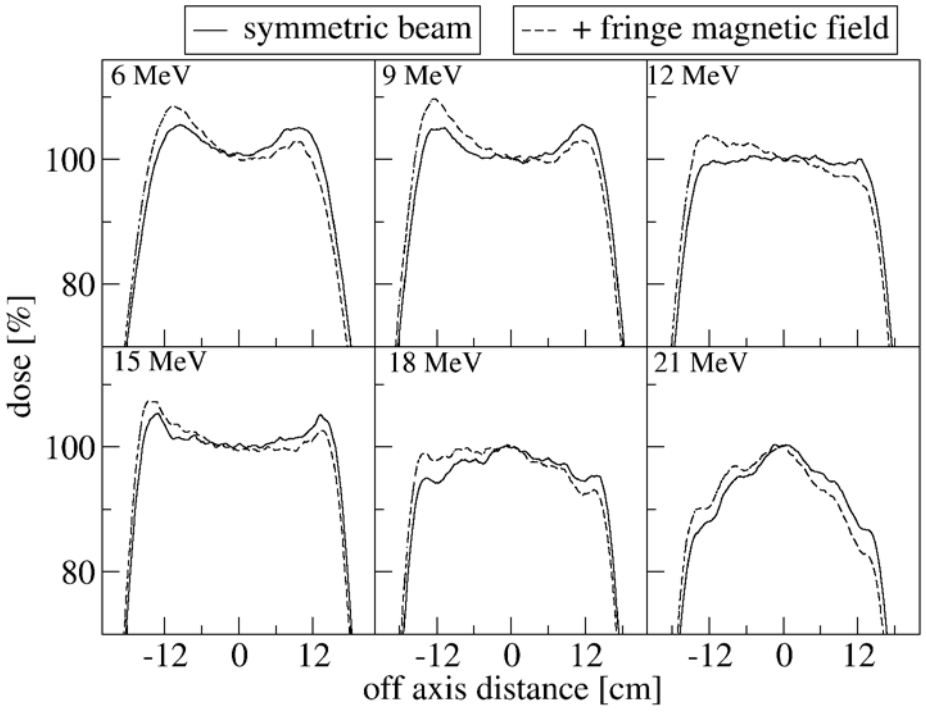

Figure 10. The effect of the simulated fringe magnetic field on symmetric dose profiles (which contain no sources of asymmetry) for 6 – 21 MeV beams and 40×40 cm^2 field size. Effects are quantified in table 1.

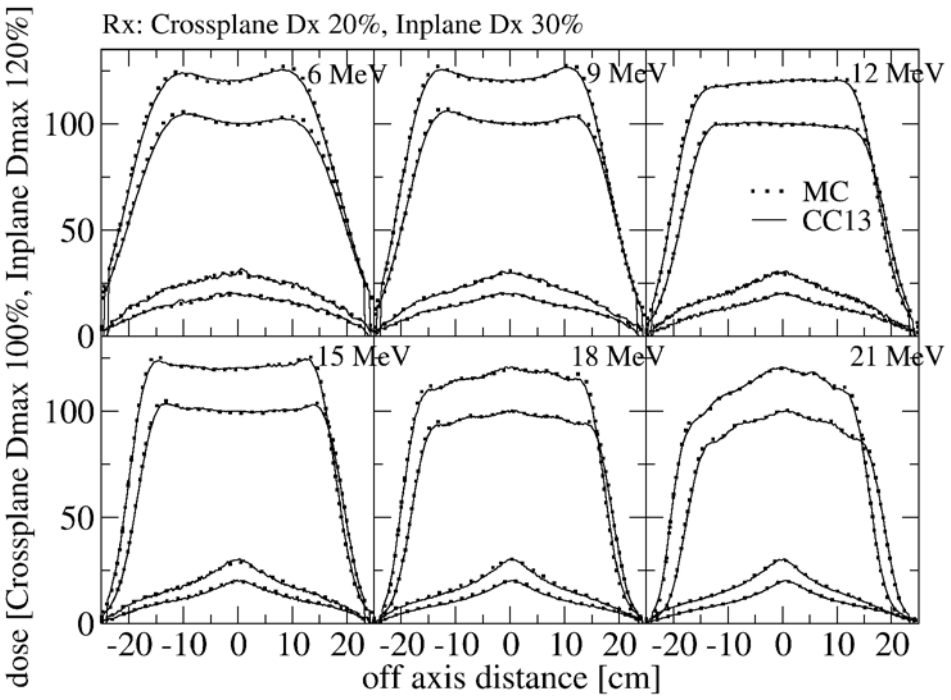

Figure 11. Comparison of Monte Carlo calculated and CC13 measured dose profiles for clinical beam 6 – 21 MeV and 40×40 cm^2 field size at 100 cm SSD.